Acta Neuropathologica Communications https://doi.org/10.1186/s40478-026-02306-x

Article in Press

High-plex spatial protein profiling of skeletal muscle biopsies in inflammatory myopathies using the MACSima™ imaging platform: A pilot study

Received: 26 February 2026

Accepted: 21 April 2026

Published online: 02 May 2026

Cite this article as: Sciacco M., Velardo D., Bertolasi L. *et al.* High-plex spatial protein profiling of skeletal muscle biopsies in inflammatory myopathies using the MACSima™ imaging platform: A pilot study. *acta neuropathol commun* (2026). https://doi.org/10.1186/s40478-026-02306-x

Monica Sciacco, Daniele Velardo, Letizia Bertolasi, Patrizia Ciscato, Giuseppe Castellano, Deborah Mattinzoli, Masami Ikehata, Stefania Corti, Giacomo Pietro Comi & Simona Zanotti

High-plex spatial protein profiling of skeletal muscle biopsies in inflammatory myopathies using the MACSima™ imaging platform: A pilot study

Monica Sciacco[1], Daniele Velardo[1], Letizia Bertolasi[1], Patrizia Ciscato[1], Giuseppe Castellano [4,5], Deborah Mattinzoli[5], Masami Ikehata[5], Stefania Corti[1,2], Giacomo Pietro Comi[2,3], Simona Zanotti[1]

[1] Neuromuscular and Rare Disease Unit, Fondazione IRCCS Ca' Granda Ospedale Maggiore Policlinico, 20122 Milan, Italy
[2] Neurology Unit, Fondazione IRCCS Ca' Granda Ospedale Maggiore Policlinico, 20122 Milan, Italy
[3] Dino Ferrari Centre, Department of Pathophysiology and Transplantation (DEPT), University of Milan, 20122 Milan, Italy
[4] Department of Clinical Sciences and Community Health, University of Milan, Milan, Italy
[5] Unit of Nephrology, Dialysis and Renal Transplantation, Fondazione IRCCS Ca' Granda Ospedale Policlinico, Milan, Italy

Corresponding author:
Simona Zanotti, simona.zanotti@policlinico.mi.it

Abstract

Inflammatory myopathies represent a heterogeneous group of autoimmune disorders affecting skeletal muscle, with distinct pathological features. While muscle biopsy remains a key diagnostic tool, conventional immunohistochemical approaches are limited in both number of available markers and spatial resolution. To explore the feasibility and potential of the MACSima™ Imaging Platform for high-dimensional, spatially resolved analysis of skeletal muscle tissue in inflammatory myopathies, we applied a panel of antibodies targeting immune cells, extracellular matrix components, blood vessels, and lymphatic markers to skeletal muscle cryosections from patients with different inflammatory myopathies and age-matched controls. Using the MACSima™ platform, we performed iterative immunofluorescence staining and imaging cycles to generate multiplexed protein maps.

The platform enabled robust signal acquisition and preserved tissue morphology throughout all cycles. Preliminary spatial analysis revealed distinct immune cell infiltration patterns, ECM remodeling signatures, and vascular changes across disease subtypes.

This pilot study demonstrates the feasibility of applying high-dimensional multiplex imaging to skeletal muscle using the MACSima™ system. Our results represent a first partial spatial profiling of muscle pathology in autoimmune myopathies using an innovative methodological approach.

Keywords: High-plex spatial protein, inflammatory myopathy, multiplex, imaging

1. Introduction

Idiopathic inflammatory myopathies (IIMs), generally indicated as myositis, refer to a diverse set of autoimmune disorders characterized by muscle weakness, inflammation, and varying degrees of muscle degeneration accompanied by various clinical manifestations affecting skin, lungs, and joints, along with the production of autoantibodies [1]. Clinically, patients often present proximal muscle weakness affecting both upper and lower limbs, myalgia and elevated serum creatine kinase (CK) levels, with the notable exception of inclusion body myositis (IBM), where CK elevation may be modest. Diagnosis generally relies on clinical examination, imaging studies, electromyography (EMG), serological testing and muscle biopsy [2]. Recent advances in targeted therapies—including interferon pathway inhibition [3,4], plasma cell–directed treatments [5], as well as innovative approaches such as CAR T-cell therapies [6,7] and bispecific antibodies [8]—are demonstrating increasing specificity and promising clinical efficacy.

Major IIM subtypes include dermatomyositis (DM), immune-mediated necrotizing myopathies (IMNM), overlap syndromes (OS), anti-synthetase syndrome (ASyS), and inclusion body myositis (IBM). DM is characterized by complement-mediated microangiopathy and perifascicular atrophy, whereas IMNM—including anti-HMGCR and anti-SRP myopathies—is primarily defined by myofiber necrosis. ASyS and OM display overlapping features with connective tissue diseases and distinct autoantibody profiles. In contrast, IBM combines chronic cytotoxic T cell–mediated inflammation with degenerative changes such as protein aggregation and impaired proteostasis, is typically refractory to immunosuppressive therapies [9-11], and likely arises from a multifactorial interplay between immune and degenerative mechanisms.

Despite significant advances in unraveling the immunopathogenesis of these disorders, the molecular determinants that confer specificity to each subtype remain incompletely elucidated.

HMGCR-Positive Myopathy (HMGCR) is characterized by symmetric proximal weakness, often, but not always, associated with statin use, and defined by autoantibodies against HMGCR (HMG-CoA reductase); muscle biopsy shows myofiber necrosis and

regeneration, endomysial CD68+ macrophage-rich infiltrates, and increased MHC class I expression [12,13].

Dermatomyositis (DM) presents with symmetric proximal weakness and characteristic skin manifestations (heliotrope rash, Gottron's papules), possible dysphagia, malignancy risk, and cardiac involvement; perivascular and perimysial CD4+ T and B cell infiltrates, complement (C5b-9) deposition, and perifascicular atrophy [14] are the main features at muscle biopsy.

Overlap Syndromes (OS) combine features of both inflammatory myopathies and connective tissue diseases, muscle biopsy findings are heterogeneous, including mixed T and B cell infiltrates, myofiber necrosis and regeneration, and variable vascular involvement [9].

Inclusion Body Myositis (IBM) typically affects adults over 50, with slowly progressive, asymmetric weakness of finger flexors and quadriceps, often with associated dysphagia; muscle biopsy shows endomysial CD8+ T cell invasion of non-necrotic fibers, rimmed vacuoles and fiber size variability [15].

The pathogenic processes in inflammatory myopathies are multifaceted, involving a complex interplay between immune-mediated injury, remodeling of the extracellular matrix (ECM), capillary network alterations, and direct disruption of muscle fiber architecture and function. However, each myositis subtype is characterized by distinctive molecular and cellular signatures.

In IMNMs, myofiber necrosis is thought to be driven by autoantibody-mediated complement activation and membrane attack complex (MAC) deposition on muscle fibers [16]. Overlap myositis exhibits heterogeneous inflammatory patterns, including perivascular and endomysial infiltrates, sometimes accompanied by vasculopathy and fibrosis [17]. In contrast, IBM is characterized by a dual pathogenic mechanism in which chronic cytotoxic T cell–mediated inflammation coexists with degenerative processes, including protein aggregation, rimmed vacuoles, mitochondrial abnormalities [18], NLRP3 inflammasome activation [19] and progressive myofiber loss [20]. Disrupted proteostasis, including impaired autophagy and protein quality control, further contributes to disease progression [21].

Advances in spatial transcriptomics have revealed previously unrecognized heterogeneity within inflammatory and degenerative zones of IBM muscle, highlighting spatial compartmentalization of pathology. Using single-nucleus RNA sequencing and spatial transcriptomics, Wischnewski et al. (2024) [20] identified selective vulnerability of type 2 myofibers, associated with localized cytotoxic T cell and type 1 dendritic cell infiltration, activation of stress markers (GADD45A, NORAD), protein degradation pathways (RNF7, p62 aggregates) and increased ACHE expression, consistent with

functional denervation. These findings define distinct molecular states in degenerating fibers and the interplay of immune-mediated inflammation, cellular stress, and denervation in IBM pathogenesis. This combination of immune dysregulation and impaired protein homeostasis drives relentless disease progression, resistant to conventional immunosuppressive therapies. Kleefeld et al. (2026) [22] further identified a disease-specific proteomic signature integrating immune and degenerative mechanisms, providing evidence that polymyositis with mitochondrial pathology (PM-Mito) may represent an early stage within the IBM spectrum. Recent clinical trials have explored targeted therapeutic approaches, including anti-IL-1 receptor [23] and molecular chaperone inducers [24], but definitive disease-modifying treatments for IBM remain elusive.

Muscle biopsy remains central for diagnosis, enabling the evaluation of inflammatory infiltrates, fiber necrosis, and microvascular alterations. However, traditional histopathological and immunohistochemical approaches are limited by the number of markers that can be assessed simultaneously, as well as by the lack of spatial resolution needed to interrogate the tissue microenvironment in detail. Mass spectrometry (MS)-based spatial proteomic approaches, including laser microdissection, MALDI imaging, and single-fiber analyses, have been widely applied to human skeletal muscle. These methods enable the quantification of hundreds to thousands of proteins and allow fiber-type–specific profiling, as demonstrated by large-scale and single-fiber studies [25-27]. While they provide deep molecular coverage and quantitative insights, they differ from antibody-based imaging platforms in spatial resolution and in the ability to directly visualize protein co-localization at the single-cell level and very low abundance proteins. Recent advances in multiplex imaging platforms have revolutionized tissue-based research by enabling the simultaneous visualization of dozens of proteins within a single tissue section while preserving spatial context. Among these, the MACSima™ Imaging Platform is an automated, high-throughput cyclic immunofluorescence system that allows the iterative staining, and imaging and signal removal of dozens of markers on the same tissue section, thereby preserving spatial context while achieving high-dimensional protein profiling. This approach allows the comprehensive characterization of cellular phenotypes, tissue architecture, and cell–cell interactions at subcellular resolution. While this technology has been successfully applied to tumor [28, 29] and lymphoid tissues [30], its application to skeletal muscle, particularly in the context of inflammatory myopathies, remains unexplored.

In this pilot study, we aimed to apply the MACSima™ platform to skeletal muscle biopsies from patients with different forms of inflammatory myopathies and controls. Our objectives were: (1) to evaluate the technical feasibility and reproducibility of the

platform in muscle tissue and (2) to explore spatial patterns of proteins associated with muscle structure, extracellular matrix modulation, inflammatory processes, and lymphangiogenesis.

2. Materials and Methods

2.1 Patients

The patient cohort was composed of 16 patients and 4 age-matched controls, the latter being individuals who had undergone skeletal muscle biopsy for suspected neuromuscular disease, but whose biopsy had turned out normal. Muscle biopsies were performed at the biceps brachii except for three patients for whom quadriceps muscle was preferred. The patients are subdivided into four pathological groups: HMGCR-statin related myositis (HMGCR), dermatomyositis (DM), overlap syndrome (OS) and inclusion body myositis (IBM). All patients were recruited from the Neurology-Neuromuscular and Rare Disease Unit of Fondazione IRCCS Ca' Granda Ospedale Maggiore Policlinico of Milano. The study was conducted in compliance with the ethical standards outlined in the Declaration of Helsinki, as well as national legislation and institutional guidelines. All participating subjects provided written informed consent, which had been approved by the local Ethical Committee, to undergo skeletal muscle biopsy, as well as storage, analysis, and collection of their data, including clinical information.

2.2 Muscle biopsy

Muscle biopsies were initially performed as part of routine diagnostics and were reassessed for the purpose of this study. Patient biopsies were selected based on clinical and serological diagnoses to represent each disease entity. Due to disease heterogeneity and sampling limitations, individual biopsies may not display all classical histopathological features.

Tissue specimens were frozen in isopentane-cooled liquid nitrogen and processed according to standard techniques. For histological analysis, 8 µm-thick cryosections were picked and processed for routine staining with Hematoxylin and Eosin (H&E), Modified Gomori Trichrome (MGT), myosin ATPase (pH 9.4-4.6-4.3), cytochrome c oxidase (COX), succinate dehydrogenase (SDH), and NADH-Tetrazolium reductase (NADH-TR). The number of necrotic fibers was counted on MGT-stained muscle sections and the percentage of necroses was calculated considering the number of fibers in each field. On the H&E-stained muscle sections, the fibrotic area (connective and adipose tissue) was quantified using Leica Application Suite 4.9.0 and ImageJ 1.53c

(https://imagej.nih.gov/ij/download.html) software. The percentage of fibers with internalized nuclei was evaluated on H&E-stained muscle sections. For all analyses, on each section, four randomly, non-overlapping, selected fields were photographed at 20X objective, using optical microscope Leica DC200 equipped with camera and IM50 image analysis software (Leica Microsystems, Wetzlar, Germany).

2.3 Tissue preparation for MACSima™ platform

The MACSima platform allows high-plex spatial analysis of tissue, enabling the simultaneous detection of multiple biomarkers within the same tissue section. For MACSima experiments three patients from each pathological group were analyzed. Preliminary H&E staining was performed on the selected muscles (Fig. 1S, Supplementary).

8 µm-thick cryostat muscle sections were mounted onto a Super Frost plus slide and fixed with cold acetone for 3 min. at -20°C. After short air drying, the MACSwell ™ Four Imaging Frame (Miltenyi Biotech, Bergisch Gladbach, Germany) was mounted on the slide that were washed three times with MACSima ™ Running Buffer (Miltenyi Biotech) until initial DAPI staining using MACSima Stain Support Kit (Miltenyi Biotech). After 10 mins of incubation at room temperature, the samples were washed three times with Running Buffer and covered with the final sample volume. Antibodies staining and washing were performed in 250 µl of volume. MACSwell ™ Four Imaging Frame were sealed with MACSwell Sealing Foil (Miltenyi Biotec) to avoid evaporation.

Antibodies were prepared in a MACSwell™ Deepwell Plate (Miltenyi Biotec) in the appropriate dilution with MACSima™ Running Buffer. Before being used, the antibodies were spinned for 20 sec at 1000 x g to sediment possible precipitates. DAPI was added to the antibody-containing Deepwell Plate in a 1:50 dilution in every eighth antibody cycle. The acquired image datasets were utilized for subsequent image processing performed in MACS iQ View Software (Miltenyi Biotec). The antibodies panel applied on MACSima platform, and the experimental conditions are reported in Table 1 Supplementary.

2.4 MICS imagining

The antibodies were incubated, as reported in Table 1S, for a variable time established in a preliminary experiment. A detailed description of the MACSima™ hardware (liquid handling system, microscope, stage) was published previously [28].

Before the iterative cycles were initiated, ROIs were defined, and the focus was adjusted. ROIs were defined based on the DAPI signal shown in the overview scan. A detailed description of images acquisition was reported by Scheuermann (2024) [29].

The acquired images were utilized for subsequent image processing performed in MACS iQ View (Miltenyi Biotec).

Advanced cell segmentation was performed using MACS iQ View segmentation pipeline and conducted on nuclear (DAPI) and cytoplasmic markers (wheat germ agglutinin, WGA and Vimentin) on whole muscle section. For nuclear segmentation the “Advanced morphology for Tissue” nuclear detection was used (Parameters: Min/Max Diameter=20/70 pixels; Detection Sensitivity=150%; Separation Force=50%; Smoothing Filters Sigma=1). Cytoplasmic segmentation was performed using the “Constrained Donut” option based on WGA and Vimentin channels (Parameters: Detection sensitivity=100%; Donut Width=10 pixels). The accuracy of the segmentation was confirmed by observing the segmentation image using the MACS iQ View software (Fig 2S, Supplementary).

2.5 Immunofluorescent staining microscope

For validation immunofluorescence staining, 8 µm-thick muscle cryosections were fixed with acetone for 3 min, washed three times with PBS, permeabilized with 0.1% Triton-X100 in PBS for 15 min., blocked with 1% normal goat serum (Vector Laboratories, Newark, CA, USA) diluted in PBS for 30 min at room temperature (RT) and incubated overnight with selected conjugated primary antibodies (Miltenyi Biotec). Following three washing with PBS, slides were mounted with antifade mounting medium with DAPI (Vectashield, Vector Laboratories). Laminin-α2 rabbit polyclonal antibody (diluted 1:200; Sigma, St. Louise, MO, USA) was used to detected sarcolemma. Leica Application Suite V4.6.2 software was used for image acquisition.

2.6 Data processing

After cell segmentation using MACS iQ View, expression data for each marker were exported as a CSV file for the normalization step. We applied winsorization to the raw expression data to mitigate the impact of potential outliers, capping values at the 1st and 99th percentiles, separately for each marker analyzed. Then, to winsorized data were applied the inverse hyperbolic sine transformation (arcsinh transformation). The normalized data were used for subsequent analysis. Graphs were produced using GraphPad Prism (Version 10.1.2) and images were exported from MACS iQ View (Version 1.2.2).

2.7 Statistical analysis

Quantitative data are shown as bar graphs, violin plots or scatter plots. Clinical and morphological data are expressed as mean ± SEM. Mann Whitney U non-parametric

testing was used for all two-group comparisons and Kruskal-Wallis test for multiple testing was used for the comparisons involving more than two groups. One-way ANOVA with QQPlot was performed to evaluate normal distribution of each marker. A one-sample t-test was performed to evaluate the statistical significance of Log (2fold change (FC)) for each protein analyzed among patients and controls. Relationships between continuous variables were assessed using nonparametric Spearman correlation. P-values ≤0.001** and ≤0.05* were considered statistically significant.

High-dimensional proteomic data were analyzed in R (v4.5.3). Features with zero variance or missing values were excluded, and data were normalized using unit variance scaling. Principal Component Analysis (PCA; *prcomp*) assessed global variance and identified major contributing markers, while non-linear relationships were explored with UMAP (*uwot* package, n_neighbors = 30, min_dist = 0.3). Unsupervised clustering was performed using K-means on UMAP coordinates, and cluster composition was used to assess diagnostic enrichment.

Gene Ontology (GO) enrichment analysis was conducted using STRING (v11.5) [31] and the *clusterProfiler* R package [32], focusing on Biological Processes. Significantly enriched terms were identified using an FDR-adjusted p-value <0.05 (Benjamini–Hochberg correction) and further filtered by protein count and fold enrichment. Concept network plots (Cnetplots) visualized functional relationships between key proteins and enriched pathways. Statistical graphics and visualizations were generated with *ggplot2*, *factoextra*, *pheatmap*, and *enrichplot.*

Biological identities were assigned to clusters by analyzing lineage-specific marker enrichment via heatmaps and violin plots. Tissue composition was quantified as the relative proportion of each identified cell population within diagnostic groups, expressed as a percentage of total cells per group.

3. Results

3.1 *Clinical aspects*

The 16 patients were subdivided into four groups each composed of four patients: HMGCR seropositive (HMGCR), dermatomyositis (DM), overlap syndrome (OS) and inclusion body myositis (IBM).

Hyposthenia, cramps, fatigability and dysphagia were among the most prevalent clinical symptoms in our patients. Extra muscular clinical manifestations involved skin in DM and OS patients (50%) and heart in one HMGCR patient. In patients who had undergone electromyography (EMG), the pattern was predominantly myopathic. Serum creatine

phosphokinase (CK) levels were increased in all patients with values ranging from 486 IU/L to 11831 IU/L (average value 6235.8 ± 4403 IU/L). More in detail, CK value was 8880 ± 3089 IU/L in HMGCR, 11831 ± 8194 IU/L in DM, 3746 ± 997 IU/L in OS and 486 ± 30 IU/L in IBM. The main demographic and clinical features are summarized in Table 1.

Table 1: Demographic and clinical characteristics of patients and controls

Demography	Ctrl	HMGCR	DM	OS	IBM
N° subjects	N=8	N=4	N=4	N=4	N=4
Female	4 (50%)	2 (50%)	2 (50%)	3 (75%)	1 (25%)
Caucasian	8 (100%)	4 (100%)	4 (100%)	4 (100%)	4 (100%)
Age at biopsy (years)	58.5 ± 5.44	71.25 ± 3.40	43.75 ± 8.03	62.5 ± 5.07	72.7 ±5.29
Disease duration (months)	-	3.0 ± 2.3	3.33 ± 3.3	48 ± 76	34 ± 27
Corticosteroid before biopsy	-	1 (33.3%)	No	No	No
Serology	-	HMGCR (1:328-1:500)	NXP2+(N=2) SAE1+ (N=1)	ANA (1:320-1:640)	-
Clinical Traits	**Ctrl**	**HMGCR**	**DM**	**OS**	**IBM**
Hyposthenia		4 (100%)	4 (100%)	4 (100%)	4 (100%)
Cramps		2 (50%)	3 (75%)	1 (33%)	1 (33%)
Myalgias		4 (100%)	4 (100%)	4 (100%)	2 (50%)
Myoglobinuria		0	0	1 (25%)	0
Dysphagia		2 (50%)	4 (100%)	2 (50%)	4 (100%)
Fatigability		4 (100%)	4 (100%)	1 (33%)	2 (50%)
Skin lesions		0	4 (100%)	2 (50%)	0
Heart		1 (33%)	0	0	0
Laboratory data	**Ctrl**	**HMGCR**	**DM**	**OS**	**IBM**
Creatine Kinase (U/L)	6-190	8880 ± 3089	11831 ± 8194	3746 ± 997	486 ± 30

Data are presented as mean ± SEM or number (%)

3.2 *Muscle biopsy*

Myopathic changes as fiber size variability and fiber splitting were present in all patients. Fibers with internalized nuclei were variably increased in all patients compared to controls, though the increase was significant only in IBM cases (5.06 ± 1.13, p=0.04) (Fig 1A). The percentage of necrotic fibers was increased in all patients compared to controls, the increase being significant only in HMGCR patients (7.93% ± 0.91%, p≤0.0001). Endo- and perimysial fibrosis was significantly increased in HMGCR (12.8% ± 1.19%, p=0.0048), DM (15.6% ± 1.51%, p=0.0001) and in IBM patients (23.7% ±

4.08%, p≤ 0.0001) compared to controls (7.49% ± 0.49%). The evaluation of cross-sectional area of fiber type showed a significant decrease of CSA for both type I and type II fibers in all patients as reported in Table 2. A significant change in % of fiber types was detected in IBM patients with a prevalence of type I (66.13% ± 4.05%, p=0.0038) vs type II (34.04% ± 1.61%, p=0.0003) compared to control type I (36.25% ± 0.63%) and type II (60.8% ± 1.07%) fibers.

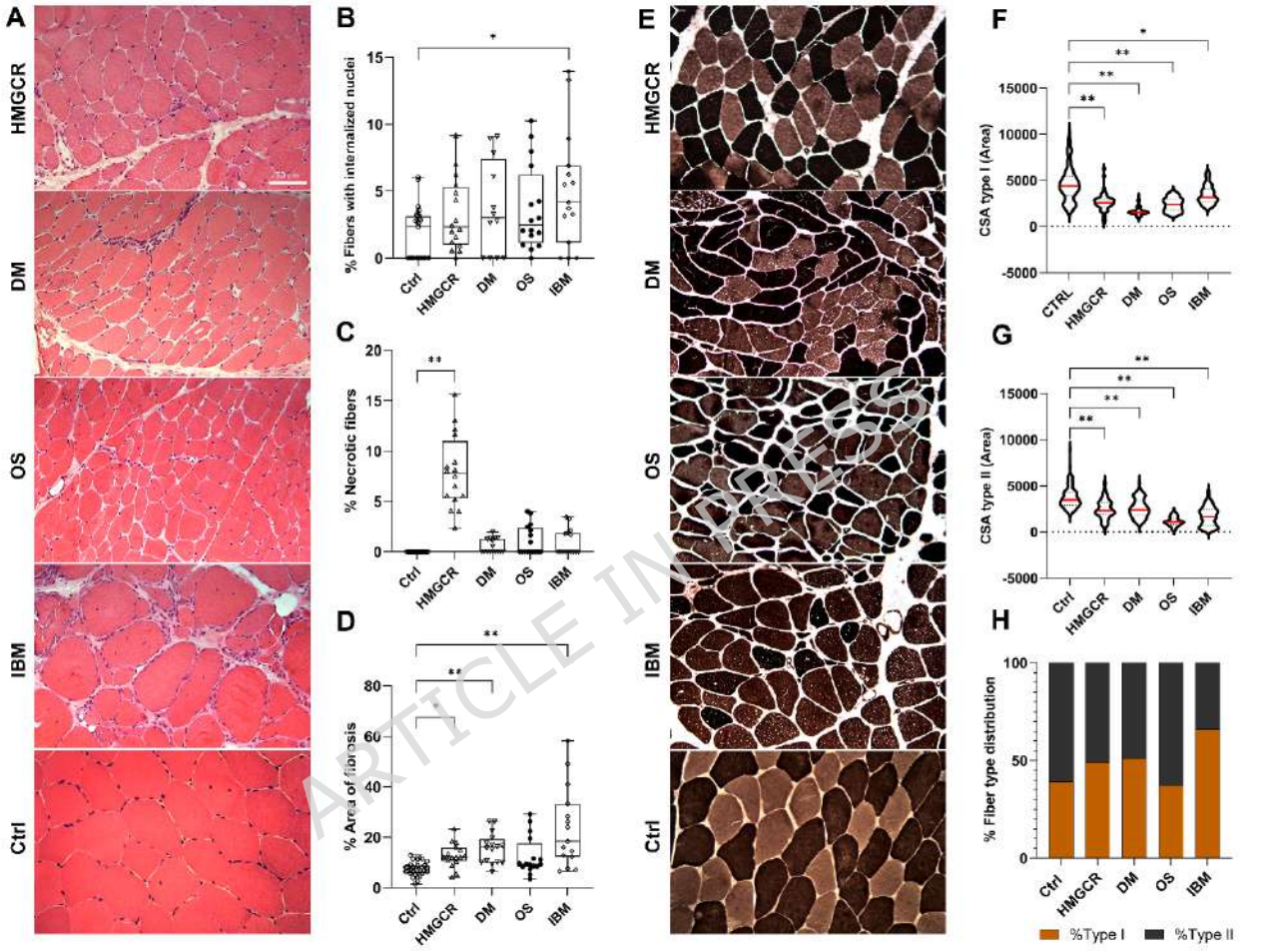

Figure 1. *A: Representative hematoxylin and eosin (H&E) stained sections from each patient group. Scale bar: 50 µm. Box plot showing the percentage of fibers with internalized nuclei (B), the percentage of necrotic fibers (C) and the percentage of fibrotic area (D). E: Representative ATPase staining at pH 9.4 from each patient group. Scale bar: 50 µm. (F) Violin plot depicting the cross-sectional area (CSA) of type I fibers (F) and of type II fibers (G). H: Stacked bar graph showing the distribution of type I and type II fibers. P-values ≤0.001** and ≤0.05* were considered statistically significant.*

Table 2: Muscle biopsy findings.

Muscle biopsy	Ctrl	HMGCR	DM	OS	IBM	p HMGCR vs DM	p HMGCR vs OS	p HMGCR vs IBM	p DM vs OS	p DM vs IBM	p OS vs IBM
% Fibers with Internalized nuclei	1.769 ± 0.354	3.210 ± 0.671	3.704 ± 1.017	3.662± 0.7986	**5.064 ± 1.132** p=0.040						
% Necrosis	0	**7.93 ± 0.91** p≤0.0001	0.558 ± 0.176	1.109 ± 0.368	0.943 ± 0.332						
% Area of fibrosis	7.49 ± 0.49	**12.8 ± 1.19** p=0.0048	**15.6 ± 1.51** p=0.0001	12.4 ± 1.90	**23.7 ± 4.08** p≤0.0001						
CSA type I (μm²)	4612 ± 180	**2605 ± 124** p≤0.0001	**1677 ± 58** p≤0.0001	**2395 ± 129** p≤0.0001	**3460 ± 96** p=0.0086	**≤0.0001**		**0.0005**	**0.014**	**≤0.0001**	**0.0003**
CSA type II (μm²)	3730 ± 110	**2464 ± 130** p≤0.0001	**2588 ± 114** p≤0.0001	**1153 ± 84** p≤0.0001	**1684 ± 99** p≤0.0001		**0.0001**	**0.0015**	**0.0001**	**0.0001**	
% Type I	36.25 ± 0.63	49.04 ± 3.74	47.45 ± 3.54	37.11 ± 4.55	**66.13 ± 4.05** p=0.0038						**0.0175**
% Type II	60.80 ± 1.07	50.96 ± 3.74	48.80 ± 1.71	62.89 ± 4.55	**34.04 ± 1.6**1 p=0.0003						**0.0033**

In bold significant data. Abbreviations: CSA cross sectional area

3.3 High-plex protein detection on MACSima™ platform

To test the panel of antibodies on MACSima platform, three selected patients from each pathological group were analyzed. The immune panel comprises 34 antibodies that were grouped for their biological role in four clusters: a “Cluster Muscle” which includes cardiac actinin (ACTC1), sarcomeric α-actinin (ACTN1), desmin (DES) and myosin-1 (MYH1); a “Cluster ECM” including collagen I (COL1A1), fibroblasts (S100A4), fibronectin (FN1), CD156c (ADAM10) and CD49b (ITGA2); a “ Cluster Inflammation” including CD3 (CD3D), CD63, CD68, CD107a (LAMP1), CD107b (LAMP2), CD206 (MRC1), CD163, CD14, CD16 (FCGR3A), CD74, HLA-ABC (HLA-DRA), HLA-DR (HLA-A), CD45 (PTPRC) TNF-α and CD254 (TNFSF11); a “Cluster Lymphangiogenesis” including CD11b (ITGAM), CD31 (PECAM), CD105 (ENG), CD106 (VCAM-1), LYVE-1, podoplanin (PDPN), CD9, CD146 (MCAM), CD171 (L1CAM) and CD201 (PROCR). The markers composing each cluster with their functional subclassification are depicted in Fig. 2.

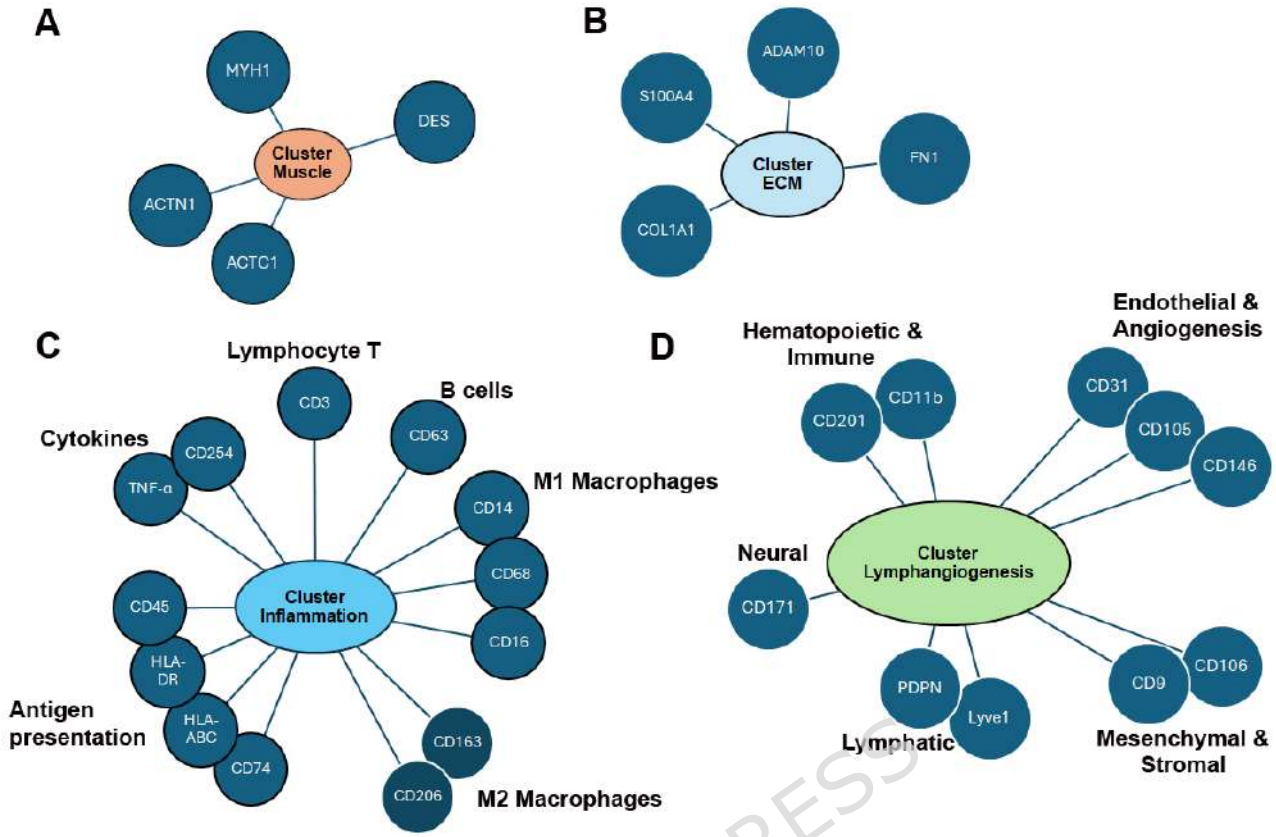

***Figure 2**: Functional classification of markers based on biological roles. Markers are grouped into clusters related to Muscle (A), Extracellular matrix (ECM) (B), Inflammation (C), and Lymphangiogenesis (D), with further subdivision of molecular markers into functional categories*.

3.3.1. Cluster Muscle

Myopathic features such as fiber size variability, splitting and necrosis were observed across all patient groups, necrosis being significantly elevated in HMGCR. While fibers with internalized nuclei were frequently detected in all subtypes, a significant increase was noted only in IBM, suggesting an inefficient or impaired regenerative response. Prominent endo- and perimysial fibrosis in HMGCR, DM, and IBM was indicative of chronic tissue remodeling. Additionally, a reduction in the cross-sectional area of both type I and type II fibers was consistently seen across all cohorts.

Notably, IBM exhibited a significant shift toward type I fiber predominance, reflecting selective loss of type II fibers. This finding aligns with the marked downregulation of MYH1, a myosin heavy chain isoform specific to type II fibers, and supports the degenerative nature of the disease. In contrast, structural protein levels in HMGCR, DM, and OS revealed upregulation of ACTC1 and ACTN1—genes associated with sarcomeric remodeling and regenerative activity—while DES (desmin) expression remained stable

across all groups, indicating preservation of intermediate filament integrity despite ongoing pathology.

Significant changes in the expression of key muscle structural proteins were detected (Fig. 3A). ACTC1 (sarcomeric actin) displayed higher fluorescence intensities in HMGCR and OS, consistent with enhanced sarcomeric remodeling. ACTN1 (α-actinin) fluorescence signal ~~expression~~ was significantly increased in HMGCR, DM, and OS, further supporting a remodeling or regenerative muscle phenotype. Conversely, MYH1 fluorescence signal was markedly downregulated in IBM, in compliance with the well-documented histopathological loss of type II fibers. DES fluorescence level remained unaltered across all disease groups, suggesting that intermediate filament architecture is maintained regardless of disease-specific alterations in sarcomeric protein levels. Collectively, these findings highlight distinct molecular signatures underlying regenerative versus degenerative muscle responses. These alterations likely reflect contributions from distinct cellular subpopulations, as later supported by single-cell proteomic analyses. Autoimmune inflammatory myopathies such as HMGCR, DM, and OS are characterized by molecular markers indicative of active regeneration and structural remodeling, whereas IBM displays a degenerative profile marked by selective fiber loss and an insufficient regenerative response.

3.3.2 Cluster ECM

ECM remodeling was prominently observed in specific disease subtypes. COL1A1 and CD156c (*ADAM10*) protein levels showed higher fluorescence intensities in HMGCR and DM, indicating increased collagen deposition and heightened ECM turnover. In DM, additional increase in fluorescence signal of S100A4, a fibroblast activation marker, and FN1 (fibronectin) was detected, supporting active fibroblast engagement and matrix deposition. In contrast, CD49b, a marker associated with integrin-mediated matrix interactions, showed no significant changes within any group.

Muscle samples from OS patients did not show substantial ECM alterations at the protein signal level, suggesting that ECM remodeling may be limited or occur in a spatially heterogeneous manner not fully captured by bulk measurements. In IBM, only COL1A1 was significantly increased, suggesting isolated collagen accumulation without broader ECM activation (Fig. 3B).

In DM, the concomitant fluorescence signal increased of S100A4 and FN1 points to profibrotic remodeling driven by activated fibroblasts. In HMGCR, ECM turnover appears to be associated with regenerative or reparative processes. Conversely, IBM demonstrated selective collagen accumulation in the absence of widespread matrix remodeling, indicating a more limited and likely non-regenerative fibrotic response.

These ECM findings further differentiate disease-specific profiles. Both HMGCR and DM displayed significant fluorescence signal increased of COL1A1 and ADAM10, with DM uniquely exhibiting elevated S100A4 and FN1, consistent with active fibroblast-mediated remodeling. In IBM, COL1A1 was isolatedly increased, while OS showed no significant ECM-related changes.

Collectively, these data underscore a clear molecular and histopathological distinction among inflammatory myopathies. HMGCR, DM, and OS exhibit molecular signatures consistent with inflammation-driven regeneration and structural remodeling. In contrast, IBM is defined by selective myofiber degeneration, impaired regenerative capacity, and minimal ECM activation, highlighting fundamentally distinct underlying pathophysiological mechanisms across these disease entities.

3.3.3 Cluster Inflammation

The most extensive alterations in inflammatory marker protein signals were seen in HMGCR-associated myopathy. Proteins displaying higher fluorescence intensities included T-cell markers (CD3), macrophage-associated antigens (CD68, CD206), lysosomal degranulation markers (CD107b), monocyte markers (CD14), MHC class I and II molecules (HLA-ABC, HLA-DR), pro-inflammatory cytokines (TNF-α), and antigen presentation molecules (CD74, CD45). This profile suggests robust activation of both innate and adaptive immune responses, characterized by antigen presentation, T-cell infiltration, and macrophage activation (Fig. 3C). Although HMGCR displays the most extensive molecular activation of inflammatory markers, this does not necessarily reflect the overall abundance of immune cells within the tissue, as further clarified by single-cell analyses, suggesting higher activation state per cell rather than increased cell number. As for the other myopathy subtypes, IBM demonstrated a similarly prominent inflammatory profile, with increased expression of overlapping markers such as CD3, CD107a/b, CD14, HLA-ABC, HLA-DR, TNF-α, and CD45. In contrast to HMGCR, this profile in IBM is associated with a higher proportion of immune cell populations, indicating a distinct inflammatory pattern characterized by cellular infiltration rather than predominantly molecular activation. Notably, CD163 was also elevated, indicating the presence of alternatively activated macrophages and a potential role for chronic inflammation and tissue remodeling (Fig. 3C).

In contrast, DM and OS showed comparatively fewer changes in inflammatory marker expression. This suggests either a lower degree of immune cell infiltration or a predominance of alternative pathogenic mechanisms, such as complement activation or interferon-mediated pathways, particularly in DM.

3.3.4 Cluster Lymphangiogenesis

The analysis of the lymphangiogenic cluster revealed substantial variability in marker expression within different pathological groups, highlighting distinct molecular profiles. A key finding is the consistent increase fluorescence signal of CD105 in HMGCR, DM, and OS. As a co-receptor for TGF-β signaling, CD105 is critically involved in vascular remodeling and angiogenesis. Its elevated expression aligns with histological evidence of neo angiogenesis in response to chronic hypoxia, and suggests an ongoing reparative or inflammatory-driven endothelial response in these conditions (Fig. 3D). Fluorescence signal of LYVE-1 was significantly increased only in DM even if its fluorescence signal was increased in all pathological groups, suggesting a key role for lymphangiogenesis and immune trafficking in the disease process, potentially contributing to both immune clearance and chronic immune activation. The increased fluorescence signal of PDPN, particularly in HMGCR and OS, further supports a shared pathogenic axis involving oxidative stress and ECM remodeling, which are likely contributors to tissue injury and fibrotic transformation (Fig. 3D).

In IBM, a distinct molecular signature emerged. Interestingly, CD9, a tetraspanin linked to muscle regeneration and immune regulation, was significantly reduced in IBM, indicating disrupted myogenic signaling, satellite cell and immune dysfunction—key features of IBM pathogenesis (Fig. 3 Box graph D). CD106 (VCAM-1) was elevated in OS, reflecting endothelial activation and facilitated leukocyte infiltration into muscle. CD171 (L1CAM), increased in IBM, may suggest neural or regenerative adaptations to chronic degeneration. CD146 (MCAM) displayed higher fluorescence intensities in both DM and IBM, which was consistent with endothelial and immune involvement. CD201 (PROCR) was significantly increased in HMGCR and OS, indicating shared endothelial-immune dysregulation linked to metabolic and autoimmune mechanisms (Fig. 3D).

Taken together, the molecular profiles point to three converging axes of disease: (1) angiogenic/endothelial remodeling (CD105, CD146), (2) oxidative and metabolic stress (PDPN, CD201), and (3) immune-muscle repair imbalance (CD9, CD171). The integration of these axes supports a refined understanding of inflammatory myopathies, where vascular and immune signatures could serve as both diagnostic biomarkers and therapeutic targets. Future studies should investigate the functional consequences following modulation of these markers, potentially guiding personalized treatment approaches.

These findings illustrate the molecular and vascular complexity of inflammatory myopathies. While HMGCR and DM are marked by active vascular remodeling and immune activation, IBM stands out with a profile dominated by chronic degeneration, compensatory angiogenesis, and impaired regeneration. OS, on the other hand, appears

to reflect a hybrid profile characterized by oxidative stress, endothelial dysfunction, and inflammation.

A summary of protein level changes and functional insights for the four groups is reported in Table 3.

Selected primary antibodies used for the analysis of the image panels were also employed for validation using the conventional immunofluorescence technique on selected patients from each pathological group. The results of single immunofluorescence staining confirmed the staining observed on MACSima™ platform (Fig. 3S Supplementary).

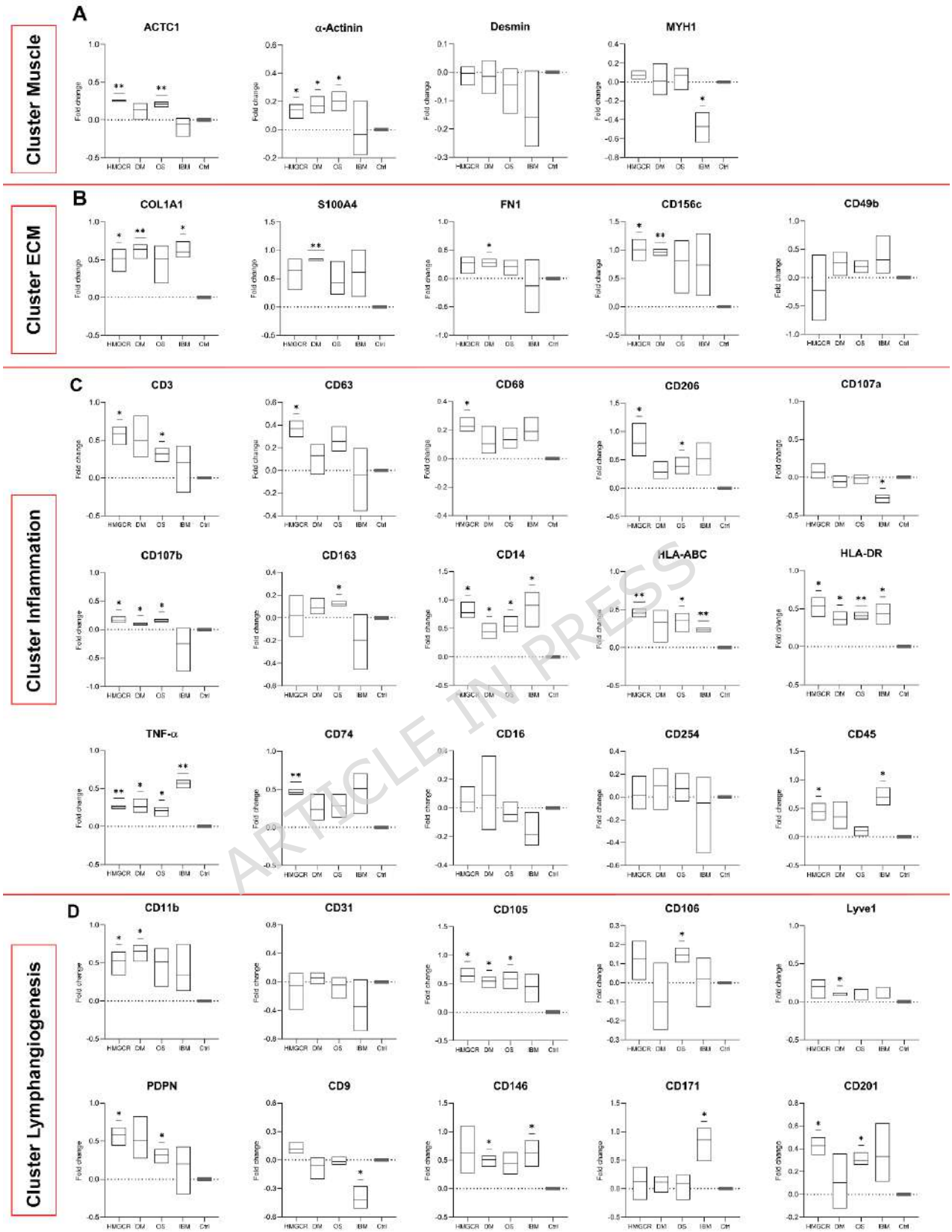

***Figure 3**: **Expression profiles of markers across experimental conditions**. Box plots show fold changes in fluorescent intensities for selected markers grouped into four functional clusters: Muscle (A), ECM (B), Inflammation (C) and lymphangiogenesis (D). Dotted lines indicate baseline expression levels. Asterisks denote statistically significant differences compared to controls: *p ≤ 0.05, **p ≤0.001.*

Table 3. Comparative molecular signatures and key functional insight for the four pathological groups for each cluster

Cluster	HMGCR	DM	OS	IBM
Muscle Structural Proteins	**↑ACTC1, ↑ACTN1**	**↑ACTN1**	**↑ACTC1, ↑ACTN1**	**↓MYH1**
Key Functional Insight	Active regeneration	Sarcomeric remodeling	Regeneration Stress adaptation	Degeneration of type II fibers

Cluster	HMGCR	DM	OS	IBM
ECM Remodeling	**↑COL1A1, ↑CD156**	**↑COL1A1, ↑S100A4, ↑CD156, ↑FN1**	**No significant changes**	**↑COL1A1**
Key Functional Insight	Matrix turnover	Fibroblast activation-Fibrosis	Minimal ECM remodeling	Mild ECM engagement

Cluster	HMGCR	DM	OS	IBM
Inflammation	**↑CD3, ↑CD63, ↑CD68, ↑CD206, ↑CD107b, ↑CD14, ↑HLA-ABC/DR, ↑CD74, ↑CD45**	**↑CD107b, ↑CD14, ↑HLA-DR**	**↑CD3, ↑CD206, ↑CD107b, ↑CD163, ↑CD14, ↑HLA-ABC/DR**	**↓CD107a, ↑CD14 ↑HLA-ABC/DR, ↑CD45**
Key Functional Insight	Robust adaptive & innate immune activation	Subtle immune involvement	Mixed immune profile	Chronic inflammation

Cluster	HMGCR	DM	OS	IBM
Lymphangiogenesis / Vascular	**↑CD11b, ↑CD105, ↑PDPN, ↑CD201**	**↑CD11b, ↑CD105, ↑Lyve1, ↑CD146**	**↑CD105, ↑CD106, ↑PDPN, ↑CD201**	**↓CD9 ↑CD146, ↑CD171,**
Key Functional Insight	Angiogenesis Metabolic stress	Vascular remodeling	Neural adaptation impaired repair Endothelial stress Inflammation	Neural adaptation impaired repair

***Table 3**: Overview of protein level changes and functional insights across the four groups. Data are grouped into functional clusters—muscle structure, ECM remodeling, inflammation, and vascular/lymphatic changes—highlighting distinct molecular signatures and disease-specific mechanisms. In red the down-regulated proteins.*

3.4 Pathway analysis

The high-plex spatial protein profiling showed the presence of 19 altered expressed proteins in HMGCR, 13 in DM, 14 in OS and 11 in IBM as shown in Venn diagram (Fig. 4A). The only protein altered in all patient groups was TNF-α. The heatmap for the protein expression of the four clusters are reported in Figure 4B. To identify enrichment pathways involved in pathogenetic mechanisms in our patients, the analysis of proteins by String database was performed.

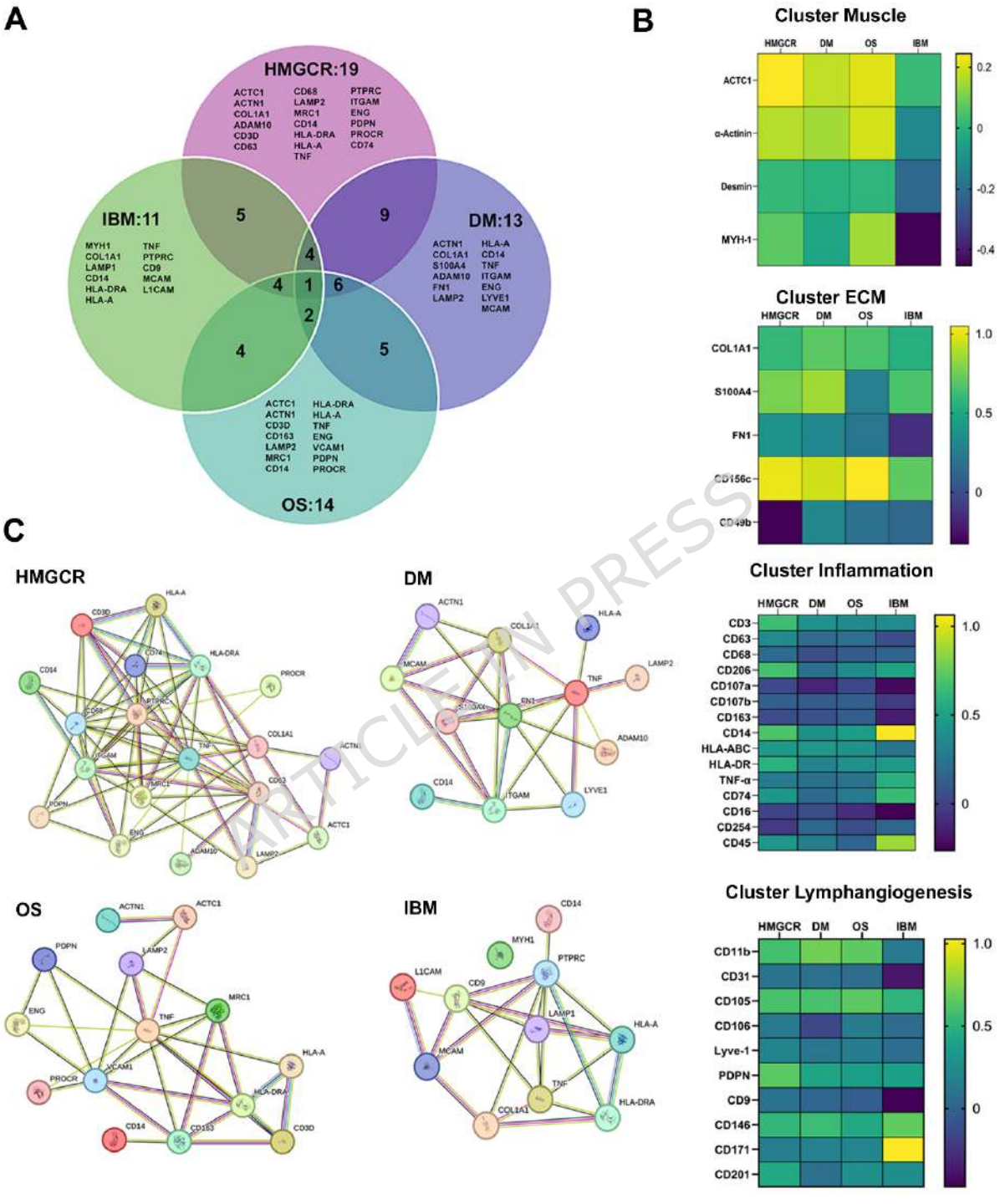

Figure 4: **Comparative analysis of protein level profiles**. *A: Venn diagram showing the distribution of differentially expressed markers in each pathological group and the overlap of differentially expressed proteins among patients' groups. B: Heatmaps showing standardized expression levels (z-score) of representative proteins grouped into functional clusters. C: Protein-protein interaction (PPI) networks of differentially expressed proteins in each pathological group, showing molecular connectivity. Networks were generated using STRING database.*

Although the number of markers in our panel is limited and does not allow for comprehensive, unbiased proteome-wide enrichment analysis, the panel was intentionally designed to target key biological processes relevant to muscle pathology. In this context, enrichment analysis should be interpreted as a hypothesis-driven, complementary approach to functionally contextualize observed marker patterns. Importantly, this targeted analysis is combined with high-resolution, spatially resolved single-cell data, providing mechanistic insights that cannot be captured by bulk or large-scale proteomic approaches.

In HMGCR, GO (Gene Ontology) analysis showed the following as the first five Biological Processes: 1) Immune system process (GO:0002376), Regulation of cell adhesion (GO:0030155), Positive regulation of response to stimulus (GO:0048584), Positive thymic T cell selection (GO:0045059), Positive regulation of leukocyte mediated cytotoxicity (GO:0001912). The first five Reactome pathways were 1) Immune system (HAS-168256), 2) Neutrophil degranulation (HAS-6798695), 3) Hemostasis (HAS-109582), 4) Adaptive Immune System (HAS-1280218), 5) Phosphorylation of CD3 and TCR zeta chains (HAS-202427) (Fig 5A). These enrichment analyses revealed a strong immunological signature in anti-HMGCR myopathy. GO Biological Process terms such as immune system process and positive regulation of response to stimulus reflect the immune activation characteristic of the disease. Enrichment in regulation of cell adhesion may relate to immune cell trafficking, while positive thymic T cell selection and positive regulation of leukocyte-mediated cytotoxicity suggest aberrant T cell development and cytotoxic activity, potentially contributing to muscle damage. Reactome pathways further support the involvement of both innate and adaptive immunity, including neutrophil degranulation and phosphorylation of CD3 and TCR zeta chains, indicative of T cell receptor signaling. Enrichment in hemostasis may reflect vascular involvement or overlapping inflammatory pathways. Altogether, these findings highlight a coordinated immune response in anti-HMGCR myopathy, involving both innate and adaptive mechanisms (Fig. 4Supplementary-A).

In DM, GO analysis identified the following as the first five Biological Processes: 1) Cell-matrix adhesion (GO:0007160), 2) Response to tumor necrosis factor (GO:0034612), 3) Positive regulation of cell migration (GO:0030335), 4) Regulation of cell migration (GO:0030335), 5) Response to wounding (GO:0009611). The first five Reactome pathways were: 1) Syndecan interactions (HAS-3000170), 2) Extracellular matrix organization (HAS-1474244), 3) Neutrophil degranulation (HAS-6798695), 4) Immune system (HAS-168256), and 5) Integrin cell surface interactions (HAS-216083) (Fig. 4Supplementary-B).

These enrichment analyses revealed strong activation of extracellular matrix remodeling and immune-related processes**.**

In OS, GO analysis showed only four Biological Processes: 1) Positive regulation of cell-cell adhesion (GO:00224093), 2) Regulation of cell adhesion (GO:0030155), 3) Immune system process (GO:0002376) and 4) Response to stress (GO:000695). The first five Reactome pathways were: 1) Adaptive immune system (HAS-1280218), 2) Immune system (HAS-168256), 3) Interferon gamma signaling (HAS-877300), 4) Antigen Processing-Cross presentation (HAS-1236975), 5) Translocation of Zap-70 to immunological synapse (HAS-202430) (Fig. 4 Supplementary-C). Enrichment analysis revealed a focused yet biologically coherent set of processes, suggesting the proteins are involved in intercellular interactions and immune responses, likely related to tissue homeostasis or inflammation. Reactome pathway analysis further supported this scenario, highlighting strong enrichment in adaptive immunity pathways, particularly T-cell activation and antigen presentation. Overall, GO and Reactome data indicate the gene set is functionally linked to immune regulation, adaptive immune responses, and mechanisms of cellular adhesion and stress response.

In IBM, GO analysis revealed the following as the first five Biological Processes 1) Positive regulation of lymphocyte mediated immunity (GO:0002708), 2) Positive regulation of adaptive immune response based on somatic (GO:0002824), 3) Regulation of cell activation (GO:0050865), 4) Positive regulation of leukocyte activation (GO:0002696) and 5) Regulation of immune response (GO:0050776). No enrichment for Reactome pathways was identified for IBM (Fig. 4 Supplementary-D).

These enrichments suggested a prominent role of adaptive immunity and immune cell activation in the pathophysiology of IBM. The enrichment of processes related to lymphocyte-mediated and leukocyte-mediated responses suggests ongoing immune activation, consistent with the chronic inflammatory features observed in muscle biopsies from IBM patients.

The enrichment analyses across pathological groups reveal a shared immunological signature dominated by adaptive immune responses—particularly T cell activation and leukocyte-mediated immunity—while also uncovering disease-specific distinctions: HMGCR and IBM exhibit strong enrichment in T cell–related processes suggestive of cytotoxic immune responses; DM is characterized by a pronounced ECM remodeling and cell migration signature reflecting tissue repair and inflammation; OS shows a more focused involvement of immune signaling and adhesion pathways, bridging features of both immune regulation and tissue stress; collectively, these findings underscore both common and divergent pathogenic mechanisms across IIMs, with immune dysregulation emerging as a common hallmark across distinct disease-specific molecular signatures.

A summary of GO and Reactome pathway enrichment results and functional interpretation across the four groups was reported in Table 2 Supplementary.

3.5 Multidimensional proteomic analysis

While initial GO and Reactome enrichment analyses provided a general biological overview, we applied Principal Component Analysis (PCA) and Uniform Manifold Approximation and Projection (UMAP) to better capture the complexity of the proteomic dataset beyond single-marker analyses. PCA revealed that the first two components explained 46.6% of the variance (Dim1: 30.4%; Dim2: 16.2%) (Fig. 5A), showing a clear separation between healthy and diseased samples. Controls clustered tightly near the origin, indicating a stable proteomic profile, whereas inflammatory myopathies displayed varying degrees of divergence. IBM showed the most pronounced shift along Dim1. DM and OS partially overlapped, indicating shared signatures, while HMGCR exhibited a distinct distribution along negative Dim2, reflecting a different cellular response. Broader dispersion in IBM and HMGCR highlights greater heterogeneity.

The PCA loading plot identified key drivers of this separation. Structural muscle proteins (ACTC1, ACTN1, MHY1) and CD9 correlated positively with Dim1 and aligned with controls. In contrast, Dim2 separated two pathological axes: a pro-inflammatory/fibrotic signature (CD3, CD68, S100A4, COL1A1) associated with IBM, and a tissue remodeling/vascular signature (FN1, CD163, CD63, CD105) associated with DM and OS. The alignment of CD3 and S100A4 suggests coordinated immune and fibrotic activity in diseased muscle (Fig.5B).

3.5.1 *Global proteomic signature and marker frequency*

High-dimensional single-cell proteomic profiling revealed distinct protein expression signatures across myopathy subtypes. In the dot plot analysis, IBM and OS exhibited broad enrichment of immune and stromal markers, with large fractions of cells expressing markers such as CD14, CD156c, CD45, Fibroblast, and FN1, indicating widespread immune infiltration and tissue remodeling. HMGCR and DM showed more selective patterns, with strong expression of specific markers (e.g., FN1, PDPN, TNF-α), but lower overall prevalence compared to IBM, whereas control samples displayed minimal expression for all markers (Fig. 5C).

Quantitative assessment of key markers confirmed these trends. IBM showed the highest proportion of CD171- and CD45-positive cells, reflecting prominent immune activation, while DM and HMGCR were characterized by elevated Fibroblast and TNF-α-positive populations. OS demonstrated intermediate enrichment across most markers. These results highlight disease-specific cellular and proteomic landscapes, suggesting

that IBM and OS are associated with more extensive immune and stromal involvement, whereas DM and HMGCR display selective immune-stromal interactions (Fig. 5D).

3.5.2 High-resolution cellular clustering and quantitative analysis of tissue architecture and cellular composition

UMAP analysis revealed a highly structured cellular landscape, with distinct clusters associated with specific pathologies. Controls showed a limited distribution, mainly within a central homeostatic cluster and a small distinct population. In contrast, inflammatory myopathies exhibited a marked expansion of diverse cellular niches. IBM displayed multiple exclusive clusters, DM and HMGCR also formed distinct populations, including a prominent DM-specific cluster, indicating that disease-associated proteomic changes arise from discrete cellular subpopulations rather than uniform tissue shifts (Fig. 5E).

Quantitative analysis of cell composition highlighted major tissue remodeling among different pathologies. Controls were dominated by healthy muscle fibers (~85%) with minimal stromal or immune components. All diseased groups showed substantial loss of muscle mass. IBM exhibited the strongest inflammatory profile, with high proportions of activated macrophages (~35%) and T cells (~30%), together exceeding half of the tissue. DM was dominated by matrix remodeling/fibrosis (~80%), consistent with a primarily structural response. HMGCR showed a heterogeneous regenerative profile, enriched in progenitor, stromal, and vascular cells, suggesting active tissue turnover. OS displayed a hybrid phenotype, combining fibrosis with a significant vascular component (Fig. 5F).

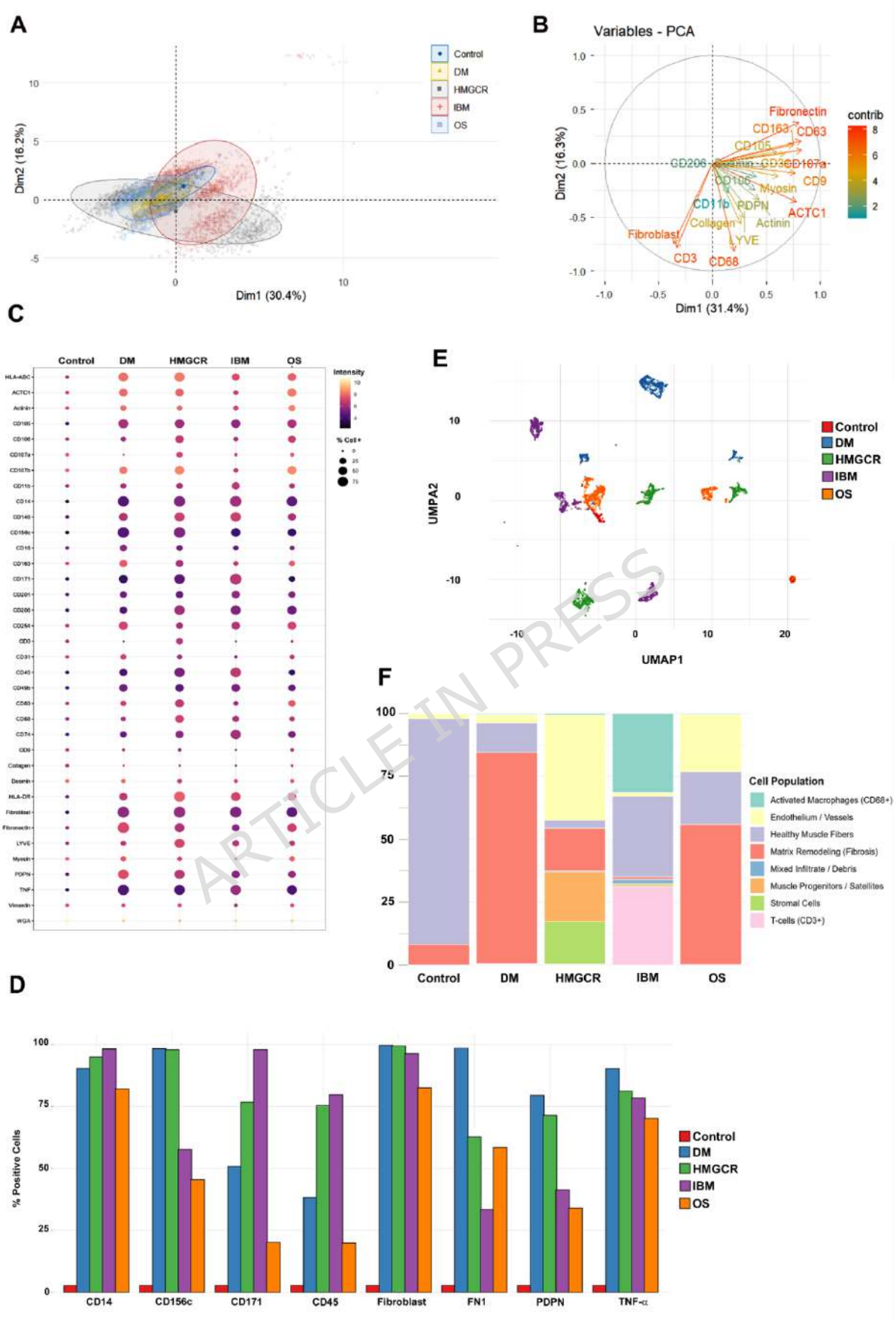

***Figure 5**. **Integration of single-cell proteomic data and cellular composition analysis**.*
(A) PCA scatter plot of single cells colored by group: Control (blue), DM (yellow), HMGCR (grey),

IBM (red), and OS (light blue). Axes represent PC1 (30.4%) and PC2 (16.2%) of variance. Ellipses (80% confidence) indicate group distributions. (B) PCA loading plot of 20 protein markers. Arrow direction indicates correlation with PCs; length and color (red–orange = high, blue–green = low) reflect contribution to variance.
(C) Integrated dot plot of protein expression across groups. Dot size represents the percentage of positive cells (>95th percentile of controls), and color (dark purple to light yellow) indicates mean fluorescence intensity (MFI). (D) Bar plot showing the percentage of cells positive for eight discriminative markers across groups (threshold: 95th percentile of control fluorescence). (E) UMAP visualization of single-cell data showing clustering by sample group: Control (red), DM (blue), HMGCR (green), IBM (purple), and OS (orange). Each point represents one cell, positioned according to phenotypic similarity based on multiplexed protein expression. Distinct clusters highlight group-specific cellular phenotypes and heterogeneity across conditions.
(F) Stacked bar plot showing the relative abundance of inferred cell populations across groups. Cell populations were defined based on marker expression profiles and include activated macrophages (CD68+), endothelium/vessels, healthy muscle fibers, matrix remodeling (fibrosis), mixed infiltrate/debris, muscle progenitors/satellites, stromal cells, and T cells (CD3+). Bars represent proportional composition within each group, illustrating disease-specific shifts in cellular architecture.

3.5.3 Functional integration of proteomic signatures

To link protein expression with biological function, we performed Gene Ontology (GO) enrichment analysis. The most significantly enriched processes included cell-matrix adhesion, cell-substrate adhesion, and wound healing (p-adjust < 0.005), primarily driven by structural markers such as Collagen and Fibronectin in DM and OS. In parallel, enrichment of acute inflammatory response and cell-cell junction organization reflected the strong immune infiltration and high expression of adhesion molecules (e.g., CD171) observed in IBM. Overall, these findings indicate coordinated tissue remodeling and sustained immune activation (Fig. 6A). Cnetplot analysis further highlighted key proteins acting as functional hubs linking multiple pathways. Two main modules emerged: an inflammatory module, centered on acute inflammatory response and driven by CD3 and CD163, and a structural module, including cell-matrix and cell-substrate adhesion. These modules were interconnected via Fibronectin, supporting a link between chronic inflammation and fibrotic remodeling in DM and OS. Additionally, a distinct cluster involving CD9 and VIM was associated with neuro-muscular interaction pathways, reflecting the unique signature of IBM (Fig 6B).

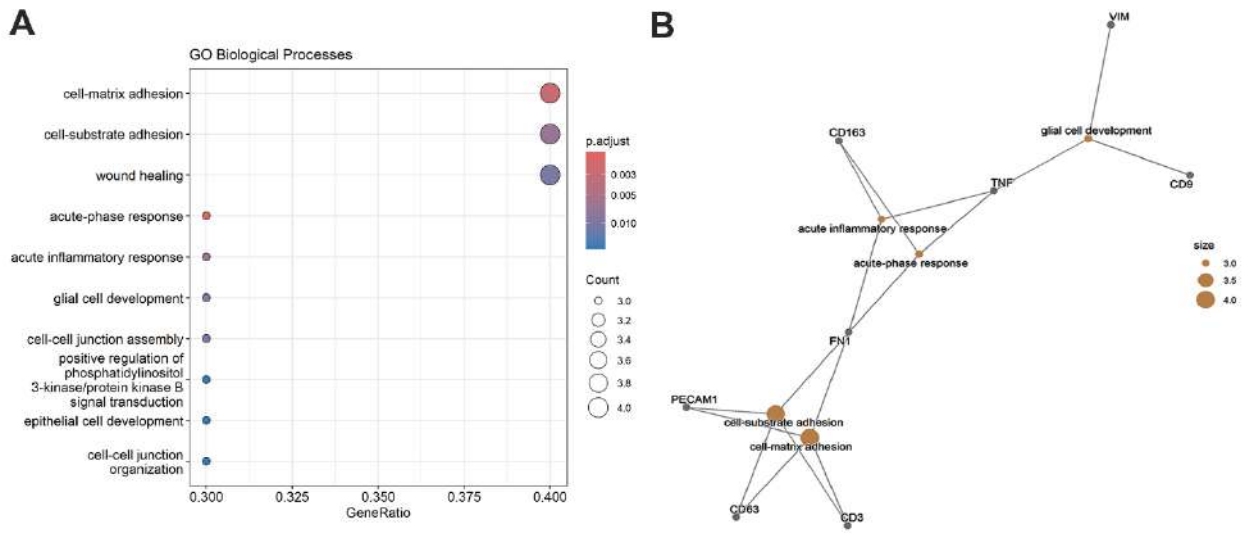

Figure 6: Interaction between differentially expressed proteins and biological pathways.
(A) Dot plot of top enriched Gene Ontology (GO) terms in the proteomic dataset. (B) Network plot showing interactions between protein markers and enriched biological processes. Orange nodes represent biological processes; grey nodes represent proteins; node size reflects the number of associated proteins. Edges indicate protein–process associations. Key proteins (e.g., TNF-α, FN1, VIM) are involved across multiple pathways, highlighting major functional axes.

In conclusion, our single-cell proteomic analysis using the MACSima™ platform provides a high-resolution map of cellular and molecular landscapes in inflammatory myopathies. PCA and UMAP indicate that disease-associated proteomic changes arise from specialized, disease-specific cellular niches. IBM emerges as a distinct immunopathological entity, characterized by the expansion of T cells and activated macrophages, with CD171 as potential diagnostic marker. In contrast, DM and HMGCR share a proteomic architecture associated with CD156c expression and matrix remodeling, suggesting stromal and vascular alterations rather than lymphocytic infiltration. Overall, these findings highlight how single-cell analysis can reveal possible disease-specific cellular signatures with potential implications for targeted therapeutic strategies.

Although the analysis integrates multilevel proteomic profiling and advanced dimensionality reduction, the limited sample size reduces statistical power, increases overfitting risk, and may not fully capture biological heterogeneity, thereby limiting generalizability. Larger cohorts are needed to validate and confirm the identified signatures and biomarkers.

3.5.4 *Integrating imaging-based proteomic signatures with clinical phenotypes*

To contextualize proteomic findings within clinical phenotypes, we integrated high-dimensional single-cell data with patient-level observations. Dimensionality reduction analyses identified distinct disease-associated patterns, reflecting the contribution of immune, stromal, and vascular compartments to pathological heterogeneity.

These signatures align with known clinical features. IBM is associated with chronic inflammation and selective fiber degeneration, supported by T-cell and macrophage expansion (CD3, CD45, CD163, CD171). In contrast, DM and HMGCR display prominent ECM remodeling and vascular adaptation (FN1, COL1A1, CD105, CD156c), consistent with regenerative and repair processes. OS exhibits a mixed immune–stromal profile, reflecting its clinical variability.

Functional enrichment analysis further supports these observations, with immune-related modules linked to inflammatory damage and ECM-related pathways associated with fibrosis and regeneration. Mapping these processes onto defined cellular populations provides a mechanistic framework connecting molecular alterations to clinical phenotypes.

A summary of marker distribution, functional clusters, and associated clinical features is reported in Table 3S Supplementary. While these results provide a detailed integrative view, methodological considerations of the MACSima™ platform compared with MS-based spatial proteomics should be taken into account.

3.6 *Limitations of the study and comparison with MS-based spatial proteomics*

While the MACSima™ Imaging Platform enables highly multiplexed, spatially resolved protein analysis at single-cell resolution, it remains a targeted, antibody-based approach with intrinsic limitations. Quantification is influenced by antibody availability, specificity, and variable affinity, and signal saturation may restrict absolute protein measurements. Panel design also constrains the breadth of proteome coverage, potentially omitting proteins or isoforms of biological relevance.

In contrast, mass spectrometry (MS)-based spatial proteomics offers a broader and more unbiased assessment of the proteome, including isoforms and post-translational modifications, and excels in global or fiber-type–specific analyses. However, MS-based approaches generally lack true single-cell spatial resolution and cannot directly visualize protein co-localization or cell–cell interactions within intact tissue. Additionally, low-abundance or cell-type–restricted proteins, such as cytokines and CD markers, may be poorly detected by MS, but are reliably captured by antibody-based imaging. Conversely, MACSima™ excels in mapping rare cell populations and in defining their spatial microenvironments (Supplementary Table 4S). Taken together, these technologies are complementary: MS-based spatial proteomics provides depth and

unbiased discovery, whereas MACSima™ affords high-resolution spatial context and sensitive detection of defined targets.

3.7 *Multiplex imaging of skeletal muscle biopsies using the MACSima™ platform*

Representative images from selected markers and patients are presented in the following panels (Figures 7-9). These images are organized by disease subtype and provide an overview of pathology-specific spatial protein fluorescent signals. They highlight the spatial complexity of inflammatory processes and structural alterations across disease groups, as revealed by the high-resolution cyclic immunofluorescence capabilities of the MACSima™ platform.

Figure 10 for a more precise characterization of tissue architecture and disease-specific microenvironments.

Figures 5S and 6S in the Supplementary section show tissue sections stained with multiple immunofluorescent markers (CD31, CD201, CD105, CD146, CD171, CD9) to highlight vascular structures, providing high-magnification views of selected regions of interest that enable detailed visualization of endothelial and perivascular components, illustrating both the distribution and potential co-localization of vascular-associated cell phenotypes and complementing the overview in

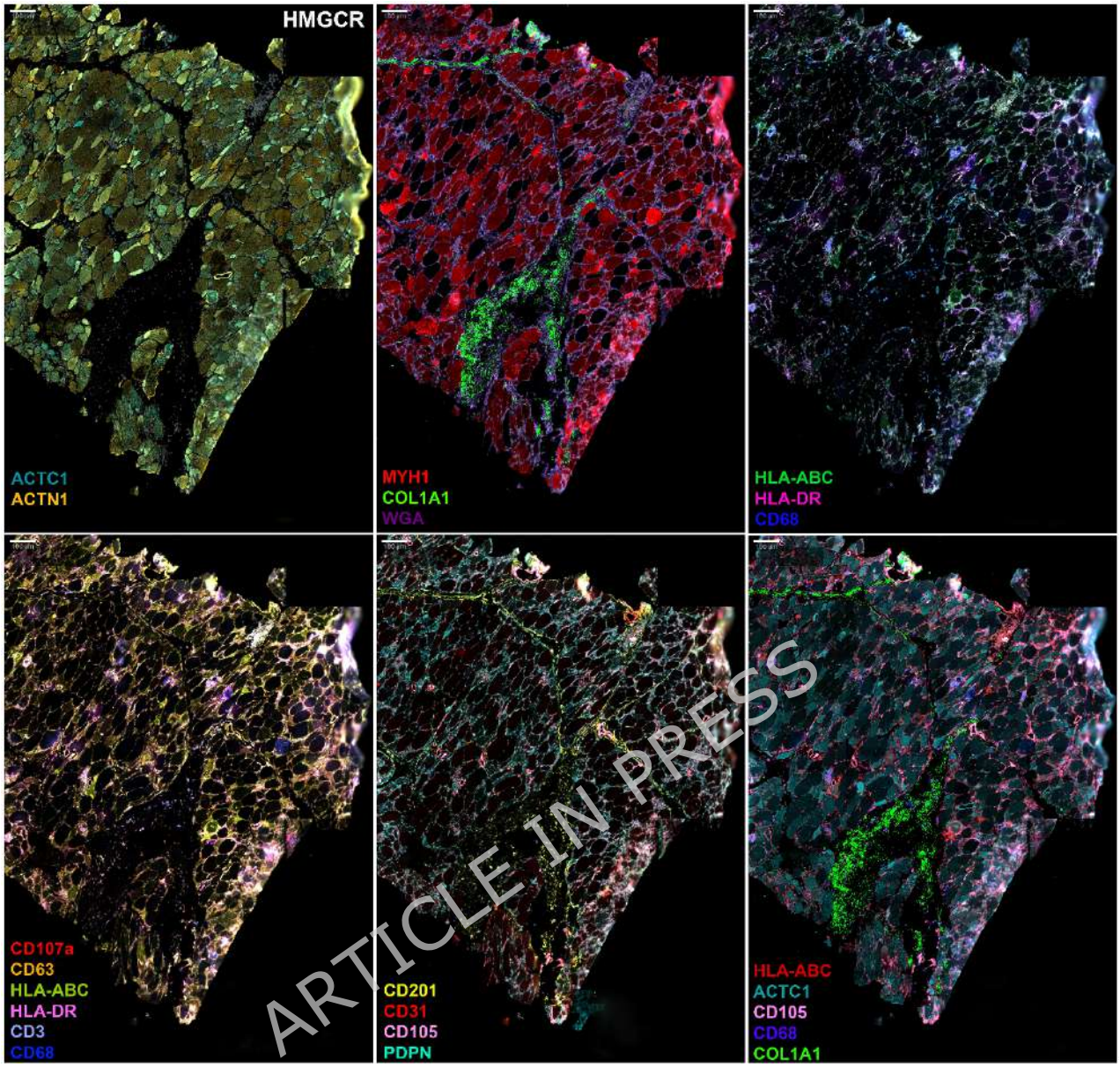

Figure 7. *Representative multiplex analysis of selected markers on whole tissue section in a HMGCR patient. Scale bar 100 µm.*

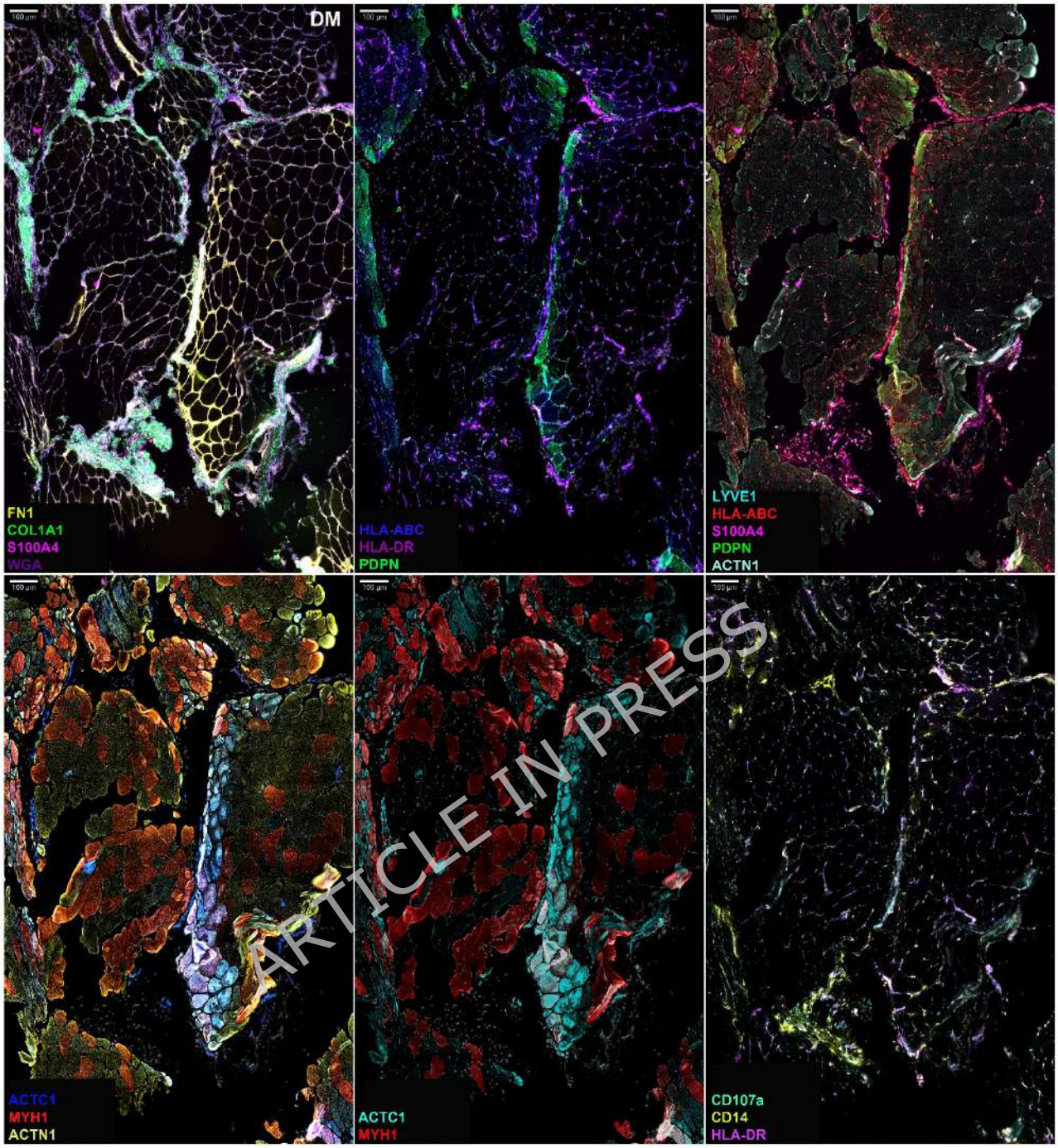

Figure 8. *Representative multiplex analysis of selected markers on whole tissue section in a DM patient. Scale bar 100 µm.*

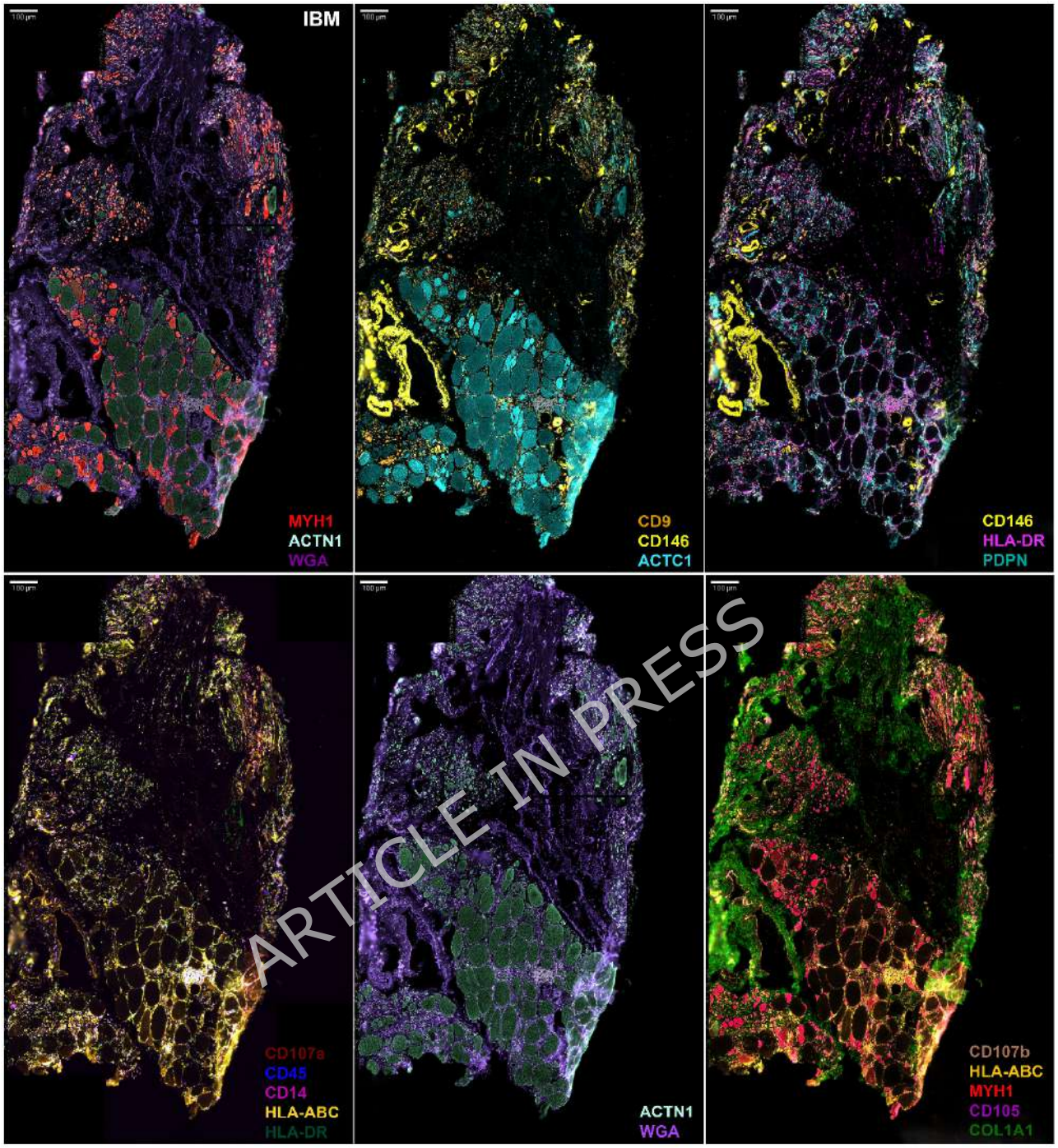

Figure 9. *Representative multiplex analysis of selected markers on whole tissue section in an IBM patient. Scale bar 100 µm.*

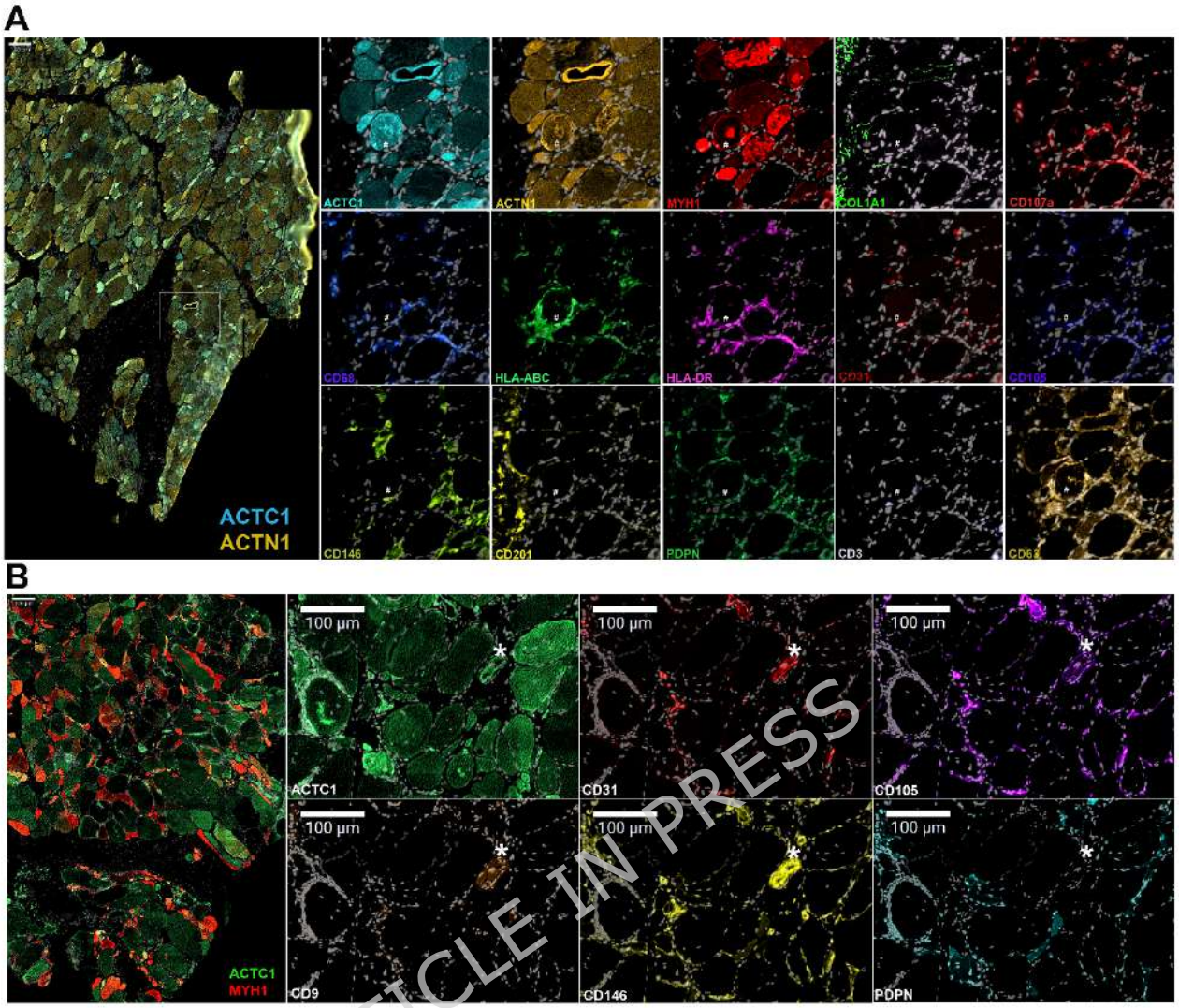

Figure 10: *Enlarged view of a muscle section from a HMGCR patient (A) showing selected markers from structural, inflammatory, and lymphangiogenic clusters. Muscle section from an IBM patient (B) highlighting selected markers from the lymphangiogenic cluster.*

4. Discussion

This pilot study provides the first comprehensive demonstration of the feasibility and biological relevance of applying high-dimensional multiplex imaging platform to human skeletal muscle tissue. By employing a custom-designed antibody panel targeting structural, immune, extracellular matrix, and vascular markers, we generated a partial high-plex protein detection profile of some IIMs. These findings highlight both the power of high-plex protein detection and the pathophysiological heterogeneity of IIMs, revealing disease-specific molecular signatures associated with inflammatory, regenerative, fibrotic, and degenerative processes. Importantly, integrating high-dimensional analytical approaches, including PCA and UMAP, extends these observations by providing a refined view of the cellular architecture underlying these

molecular signatures, offering a multi-layered perspective on disease-specific mechanisms

This comparative molecular profiling reveals distinct yet overlapping pathophysiological mechanisms within HMGCR myopathy, DM, OS, and IBM. Analysis of muscle structural proteins indicates that HMGCR and OS are characterized by upregulation of ACTC1 and ACTN1, suggesting active regeneration and sarcomeric repair. In contrast, IBM is marked by downregulation of MYH1, consistent with selective type II fiber loss. These findings support a degenerative phenotype with impaired regeneration, in line with the chronic, treatment-resistant nature of IBM [33-34]. DM shows moderate structural remodeling, primarily through ACTN1 upregulation. These structural alterations are further supported by single-cell analyses, which demonstrate that regenerative and degenerative signatures arise from distinct cellular populations rather than uniform tissue-wide changes. Interestingly, desmin levels were preserved across all subtypes, indicating that, despite sarcomeric remodeling or degeneration, the intermediate filament scaffold remains intact—highlighting a selective, rather than global, disintegration of structural components.

ECM changes further distinguished disease subtypes [35]. ECM remodeling signatures are most prominent in DM, with elevated COL1A1, S100A4, CD156 and FN1 expression, reflecting fibroblast activation and pro-fibrotic signaling. Consistently, single-cell composition analysis revealed a predominance of matrix-remodeling and fibrotic cell populations in DM, reinforcing the interpretation of ECM remodeling as a dominant pathological feature in this subtype.

HMGCR also displays increased matrix turnover, while OS shows minimal ECM changes. In contrast, the broader cellular involvement observed in OS suggests that subtle molecular ECM alterations may translate into heterogeneous tissue remodeling not fully captured by bulk protein intensity measurements.

IBM presents with mild ECM changes, potentially secondary to chronic stress. Notably, CD49b, a key integrin involved in ECM interaction, remained unchanged throughout all groups.

The inflammatory signatures revealed both shared and distinct features [36]. HMGCR exhibits robust activation of both innate and adaptive immune pathways, with broad upregulation of T cell, myeloid, and antigen-presenting cell markers. In contrast, DM demonstrates a more limited immune profile, primarily involving monocyte/macrophage markers and HLA-DR. The limited expression of cellular immune markers suggests that non-cellular immune mechanisms—such as complement activation and interferon signaling—may be more relevant in these subtypes. This is in

keeping with previous studies demonstrating the role of type I interferons and complement-mediated injury in DM pathogenesis [37]. OS displays a mixed immune signature, whereas IBM shows chronic inflammation marked by persistent antigen presentation and reduced cytolytic activity, suggesting immune exhaustion or dysregulation. Notably, integration with single-cell data refines this interpretation, revealing that while HMGCR is characterized by a strong molecular immune activation, IBM exhibits a higher abundance of immune cell populations, particularly T cells and macrophages, indicating distinct, but complementary inflammatory modalities—functional activation versus cellular infiltration. These findings support the notion that IIMs encompass distinct immunopathological entities, rather than representing a linear continuum of immune activation.

Beyond immune infiltration, our data reveal striking differences in vascular and lymphangiogenic remodeling within IIM subtypes. HMGCR and DM are associated with increased expression of angiogenic markers, indicating endothelial activation under stress or inflammatory conditions. CD105, a TGF-β co-receptor involved in endothelial activation and angiogenesis, was significantly upregulated in HMGCR, DM, and OS, indicating endothelial remodeling in response to chronic inflammation or tissue hypoxia. PDPN, a multifunctional protein implicated in lymphangiogenesis, immune regulation, and oxidative stress, was also elevated in these subtypes—most notably in HMGCR and OS—highlighting the role of redox imbalance and vascular dysfunction in disease progression. These vascular signatures are further supported by the enrichment of endothelial and stromal cell populations observed in single-cell analyses, suggesting that vascular remodeling represents a coordinated component of tissue adaptation rather than an isolated molecular event.

IBM, once again, showed a distinct vascular profile. CD9, a tetraspanin critical for myoblast fusion [38] and immune signaling [39], was significantly downregulated, pointing to impaired muscle regeneration and disrupted immune-muscle crosstalk. This aligns with the degenerative features of sIBM and its limited response to immunosuppression. Conversely, upregulation of CD171, a neural cell adhesion molecule involved in regeneration, may reflect chronic compensatory responses to degeneration [40,41].

Taken together, these data delineate a continuum of muscle disease mechanisms, ranging from immune-driven regeneration (HMGCR), to fibrosis-dominant inflammation (DM), to mixed regenerative-immune features (OS), and ultimately to chronic degenerative pathology (IBM).

Pathway enrichment analysis further contextualized these proteomic findings. HMGCR myopathy exhibited enrichment in both innate and adaptive immune responses,

including T cell receptor signaling and neutrophil degranulation, consistent with a cytotoxic immune-mediated pathology. In DM, the dominance of ECM remodeling, cell adhesion, and integrin-related pathways pointed to tissue repair and fibroblast activation. OS showed targeted enrichment in antigen presentation and interferon signaling, while IBM was characterized by pathways related to lymphocyte-mediated immunity, albeit without significant Reactome enrichment—highlighting its chronic degenerative and immune-dysregulated nature. TNF-α emerged as the only protein with higher fluorescence intensities consistently across all subtypes, underscoring its potential role as a pan-disease inflammatory mediator.

Importantly, these pathway-level findings are consistent with the cellular distributions identified through PCA and UMAP analyses, indicating that enriched biological processes arise from specific cellular subsets within the tissue microenvironment.

To further investigate disease heterogeneity, we applied high-dimensional approaches which captured the multidimensional structure of the dataset beyond single-marker analyses.

IBM was characterized by strong immune activation, with expanded T-cell and macrophage populations, whereas DM and HMGCR exhibited selective stromal and vascular remodeling. OS displayed an intermediate, hybrid phenotype combining fibrosis and vascular components. Functional integration via GO enrichment identified coordinated tissue remodeling and immune activation: inflammatory modules were linked to structural modules, suggesting interplay between chronic inflammation and fibrosis, while IBM showed a distinct neuro-muscular signature.

Overall, these findings highlight the value of multidimensional frameworks in providing an integrated view of inflammatory myopathies. In this context, single-cell resolution provides a critical link between protein expression patterns and their cellular sources, enabling a more precise interpretation of disease mechanisms.

Our results highlight the potential of spatial proteomics to identify disease-specific endotypes—regenerative, inflammatory, fibrotic, or degenerative—that may guide patient stratification and inform precision treatment strategies. This platform may also serve as a powerful tool for biomarker discovery in future longitudinal or interventional studies.

We do recognize, however, that this study has some limitations. As a pilot analysis, the sample size was limited, which may affect the statistical power of the findings. The study was cross-sectional, preventing assessment of dynamic changes over time. Although some markers were validated using conventional immunofluorescence, additional

validation (e.g., Western blotting, single-cell transcriptomics) would strengthen the findings.

A further development of the protocol will include the possibility to selectively analyze specific areas of the specimen in greater detail, such as an individual damaged fiber or a particular region rich in lymphatic or capillary vessels. Importantly, although LMD- and MALDI-based approaches already allow targeted analyses, MS-based spatial proteomics offers the added benefit of high-resolution, multiplexed molecular information in these selected regions [25, 27].

Additionally, the antibody panel applied may be expanded to more precisely investigate the inflammatory profile. The limited number of muscle biopsies examined in this pilot study limited the possibility of statistically correlating proteomic data with clinical and laboratory aspects.

Future research should include a great number of patients to integrate proteomic data with clinical phenotyping, longitudinal follow-up, and therapeutic outcomes to explore the utility of these molecular signatures in diagnosis, prognosis, and treatment stratification.

5. Conclusion

In conclusion, this study establishes the feasibility and scientific value of applying high-plex protein detection to skeletal muscle tissue. By revealing distinct molecular architectures within inflammatory myopathies—including divergent immune, regenerative, vascular, and ECM-related pathways—we offer new insights into the pathophysiological heterogeneity of these diseases. Integrating multidimensional analyses provides a more refined view of disease mechanisms by linking molecular signatures to their cellular context

The development of more detailed antibody panels for the evaluation of the inflammatory component will allow us to dissect in even more depth the pathogenetic molecular mechanisms associated with the different IMMs. These findings lay the groundwork for precision pathology approaches in neuromuscular medicine and open new avenues for biomarker development, therapeutic targeting, and individualized patient care in inflammatory myopathies.

Author Contributions:

SZ, SM-conceived the idea and revised the literature. SZ, DM, IM-interpreted the results. SZ, SM-wrote the manuscript. SM, DV-performed clinical assessment. LB, PC-performed histological studies on muscle. DM, MI, SZ-performed MACSima experiments. MS, SC,

GC and GPC-critically revised the final version of the manuscript. All the authors have read and approved the manuscript.

Funding: This work was partially supported by the Italian Ministry of Health (Ministero della Salute, Ricerca Corrente 245).

Institutional Review Board Statement: The study was conducted in accordance with the Declaration of Helsinki and approved by the Institutional Ethics Committee of the “IRCCS Ca’ Granda Foundation Ospedale Maggiore Policlinico, Italy”.

I**nformed Consent Statement:**
Written informed consent has been obtained from both patient and controls to publish this paper.

Data Availability Statement:
The data presented in this study are available on reasonable request from the corresponding author.

Acknowledgments: We thank the Associazione Centro Dino Ferrari for its support. Muscle biopsy and DNA samples were provided by the Bank of muscle tissue, peripheral nerve, DNA, and Cell Culture, member of Telethon Network of Genetic Biobanks, at Fondazione IRCCS Ca' Granda, Ospedale Maggiore Policlinico, Milano, Italy. This work was promoted within the European Reference Network (ERN) for Neuromuscular Diseases (MS as HCP Representative for the Italian ERN-NMD). The authors would like to thank the Fondazione IRCCS Ca' Granda Ospedale Maggiore Policlinico for the flagship project in the transplantation area funded with 5x1000 funds RC5100022B, "New Approaches to Spatial Proteomics in Transplantation." We thank Dr. Pedrazzini Alessandra for her outstanding technical support.

References

1. Selva-O'Callaghan A, Pinal-Fernandez I, Trallero-Araguás E, Milisenda JC, Grau-Junyent JM, Mammen AL. Classification and management of adult inflammatory myopathies. Lancet Neurol. 2018, 17(9):816-828. doi: 10.1016/S1474-4422(18)30254-0.

2. Dalakas MC. Inflammatory Muscle Diseases. N Engl J Med. 2015;373(4):393-4. doi: 10.1056/NEJMc1506827.

3. Aggarwal R, Domyslawska I, Carreira P*, et al.* Pos1207 efficacy and safety of anti-INF-β-specific monoclonal antibody, pf-06823859, on myositis: phase 2

study in patients with moderate-to-severe dermatomyositis. Annals Of the Rheumatic Diseases 2023;82**:**936-937.

4. Shaw KS, Reusch DB, Castillo RL, Hashemi KB, Sundel R, Dedeoglu F, Vleugels RA. Rapid Improvement in Recalcitrant Cutaneous Juvenile Dermatomyositis with Anifrolumab Treatment. JAMA Dermatol. 2024;160(2):237-238. doi: 10.1001/jamadermatol.2023.4744.

5. Groener M. and Paik JJ. Emerging B and plasma cell-targeting immune therapies in idiopathic inflammatory myopathies. Front. Immunol. 2025;16:1581323. doi: 10.3389/fimmu.2025.1581323

6. Muller F, Taubmann J, Bucci L, Wilhelm A, Bergamann C, Volkl S, et al., CD19 CAR-T-Cell therapy in Autoimmune Disease- A Case Series with Follow-up. N Engl J Med. 2024;390(8):687-700.

7. Cheng J, Zhang X, Fan Y, Zhang Z. CAR-T therapy for autoimmune rheumatic diseases: navigating clinical frontiers between breakthroughs and uncertainties. Clin Exp Med. 2026;26(1):177. doi: 10.1007/s10238-026-02076-9.

8. Liu T, Chen B, Yin G, Xie Q. Targeting B Cells for the Treatment of Idiopathic Inflammatory Myopathy. Clin Rev Allergy Immunol. 2025;68(1):40. doi: 10.1007/s12016-025-09047-0.

9. Salajegheh MK, Amato AA. Idiopathic Inflammatory Myopathies. Continuum (Minneap Minn). 2025;31(5):1385-1408. doi: 10.1212/cont.0000000000001617.

10. Diomedi M, Fattorini F, Aliberti S, Bianchessi LM, Castellucci A, Schmidt J, Cavagna L, Carli L, Barsotti S. Idiopathic inflammatory myopathies: one year in review 2025. Clin Exp Rheumatol. 2026;44(2):167-177. doi: 10.55563/clinexprheumatol/2z01e0.

11. Martins EF, Cappello CH, Shinjo SK, Appenzeller S, de Souza JM. Idiopathic Inflammatory Myopathies: Recent Evidence Linking Pathogenesis and Clinical Features. Int J Mol Sci. 2025;26(7):3302. doi: 10.3390/ijms26073302.

12. Cao Y, Li W, He X, Liao M, Hu K, Wu S, Zhang X, Liao Q, Shen Z, Liang Z, Zheng C, Zhong Z, Jiang H, Huang Q, Zheng H. Clinical-pathologic classification of anti-HMGCR-positive immune-mediated necrotizing myopathy. Sci Rep. 2025;15(1):34884. doi: 10.1038/s41598-025-17766-9.

13. Yoon J, Kim SW, Kim SH, Song JJ, Park YB, Park HJ, Shin HY, Park SH, Rhee Y. Clinical Characteristics and Management of Statin-Associated Anti-3-Hydroxy-3-Methylglutaryl-Coenzyme A Reductase Immune-Mediated Necrotizing Myopathy. J Clin Med. 2025;14(18):6610. doi: 10.3390/jcm14186610.

14. Treasure K, Chugh R, Abbas H, Patel A. Early detection and intervention in dermatomyositis: current evidence and clinical implications. Clin Rheumatol. 2026;45(4):2137-2148. doi: 10.1007/s10067-026-07971-w.

15. Guglielmi V, Cheli M, Tonin P, Vattemi G. Sporadic Inclusion Body Myositis at the Crossroads between Muscle Degeneration, Inflammation, and

Aging. *International Journal of Molecular Sciences*. 2024; 25(5):2742. doi.org/10.3390/ijms25052742.

16. Kurashige T. Anti-HMGCR myopathy: clinical and histopathological features, and prognosis. Curr Opin Rheumatol. 2021;33(6):554-562. doi: 10.1097/BOR.0000000000000832.

17. Silva AMS, Campos ED, Zanoteli E. Inflammatory myopathies: an update for neurologists. Arq Neuropsiquiatr. 2022;80(5 Suppl 1):238-248. doi: 10.1590/0004-282X-ANP-2022-S131

18. Kleefeld F, Cross E, Lagos D, Walli S, Schoser B, Hentschel A, Ruck T, Nelke C, Hahn K, Hathazi D, Mammen AL, Casal-Dominguez M, Gut M, Gut IG, Heath S, Schänzer A, Goebel HH, Pinal-Fernandez I, Roos A, Preuße C, Stenzel W, Horvath R. Mitochondrial damage is associated with an early immune response in inclusion body myositis. Brain. 2025;148(9):3199-3214. doi: 10.1093/brain/awaf118.

19. Naddaf E, Nguyen TKO, Watzlawik JO, Gao H, Hou X, Fiesel FC, Mandrekar J, Kokesh E, Harmsen WS, Lanza IR, Springer W, Trushina E. NLRP3 Inflammasome Activation and Altered Mitophagy Are Key Pathways in Inclusion Body Myositis. J Cachexia Sarcopenia Muscle. 2025;16(1):e13672. doi: 10.1002/jcsm.13672.

20. Wischnewski S, Thäwel T, Ikenaga C, Kocharyan A, Lerma-Martin C, Zulji A, Rausch HW, Brenner D, Thomas L, Kutza M, Wick B, Trobisch T, Preusse C, Haeussler M, Leipe J, Ludolph A, Rosenbohm A, Hoke A, Platten M, Weishaupt JH, Sommer CJ, Stenzel W, Lloyd TE, Schirmer L. Cell type mapping of inflammatory muscle diseases highlights selective myofiber vulnerability in inclusion body myositis. Nat Aging. 2024;4(7):969-983. doi: 10.1038/s43587-024-00645-9.

21. Brady S, Poulton J, Muller S. Inclusion body myositis: Correcting impaired mitochondrial and lysosomal autophagy as a potential therapeutic strategy. Autoimmun Rev. 2024;23(11):103644. doi: 10.1016/j.autrev.2024.103644.

22. Kleefeld F, Schroeter CB, Abdennebi D, Dobelmann V, Walli S, Roos A, Distler U, Tenzer S, Bopp T, Quint P, Schmitt LI, Leo M, Hagenacker T, Pinal-Fernandez I, Casal-Dominguez M, Mammen AL, Preuße C, Maggi L, Mensch A, Meuth SG, Stenzel W, Ruck T, Nelke C. Proteomic profiles in inclusion body myositis and polymyositis with mitochondrial pathology. Acta Neuropathol Commun. 2026;14(1):49. doi: 10.1186/s40478-026-02243-9.

23. Kosmidis ML, Alexopoulos H, Tzioufas AG, Dalakas MC. The effect of anakinra, an IL1 receptor antagonist, in patients with sporadic inclusion body myositis (sIBM): a small pilot study. J Neurol Sci. 2013;334(1-2):123-5. doi: 10.1016/j.jns.2013.08.007.

24. Machado PM, McDermott MP, Blaettler T, Sundgreen C, Amato AA, Ciafaloni E, Freimer M, Gibson SB, Jones SM, Levine TD, Lloyd TE, Mozaffar T, Shaibani AI, Wicklund M, Rosholm A, Carstensen TD, Bonefeld K, Jørgensen AN, Phonekeo K, Heim AJ, Herbelin L, Barohn RJ, Hanna MG, Dimachkie MM; Arimoclomol in IBM Investigator Team of the Neuromuscular Study Group. Safety and efficacy of arimoclomol for inclusion body myositis: a multicentre, randomised, double-

blind, placebo-controlled trial. Lancet Neurol. 2023;22(10):900-911. doi: 10.1016/S1474-4422(23)00275-2.

25. Murgia M, Nogara L, Baraldo M, Reggiani C, Mann M, Schiaffino S. Protein profile of fiber types in human skeletal muscle: a single-fiber proteomics study. Skelet Muscle. 2021;11(1):24. doi: 10.1186/s13395-021-00279-0.

26. Parker KC, Walsh RJ, Salajegheh M, Amato AA, Krastins B, Sarracino DA, Greenberg SA. Characterization of human skeletal muscle biopsy samples using shotgun proteomics. J Proteome Res. 2009;8(7):3265-77. doi: 10.1021/pr800873q.

27. Momenzadeh A, Jiang Y, Kreimer S, Teigen LE, Zepeda CS, Haghani A, Mastali M, Song Y, Hutton A, Parker SJ, Van Eyk JE, Sundberg CW, Meyer JG. A Complete Workflow for High Throughput Human Single Skeletal Muscle Fiber Proteomics. J Am Soc Mass Spectrom. 2023;34(9):1858-1867. doi: 10.1021/jasms.3c00072.

28. Kinkhabwala A, Herbel C, Pankratz J, Yushchenko DA, Rüberg S, Praveen P, Reiß S, Rodriguez FC, Schäfer D, Kollet J, Dittmer V, Martinez-Osuna M, Minnerup L, Reinhard C, Dzionek A, Rockel TD, Borbe S, Büscher M, Krieg J, Nederlof M, Jungblut M, Eckardt D, Hardt O, Dose C, Schumann E, Peters RP, Miltenyi S, Schmitz J, Müller W, Bosio A. MACSima imaging cyclic staining (MICS) technology reveals combinatorial target pairs for CAR T cell treatment of solid tumors. Sci Rep. 2022;12(1):1911. doi: 10.1038/s41598-022-05841-4.

29. Scheuermann S, Kristmann B, Engelmann F, Nuernbergk A, Scheuermann D, Koloseus M, Abed T, Solass W, Seitz CM. Unveiling spatial complexity in solid tumor immune microenvironments through multiplexed imaging. Front Immunol. 2024;15:1383932. doi: 10.3389/fimmu.2024.1383932.

30. Molina ISM, Okkenhaug H, Walker S, Linterman M, Marcial-Juárez E. Spatial Profiling of Germinal Centers in Mouse Secondary Lymphoid Organs Using MACSima Imaging Cyclic Staining Technology. Eur J Immunol. 2026;56(2):e70157. doi: 10.1002/eji.70157.

31. Szklarczyk D, Gable AL, Nastou KC, Lyon D, Kirsch R, Pyysalo S, Doncheva NT, Legeay M, Fang T, Bork P, Jensen LJ, von Mering C. The STRING database in 2021: customizable protein-protein networks, and functional characterization of user-uploaded gene/measurement sets. Nucleic Acids Res. 2021;49(D1):D605-D612.doi: 10.1093/nar/gkab835.

32. Yu G, Wang LG, Han Y, He QY. clusterProfiler: an R package for comparing biological themes among gene clusters. OMICS: A Journal of Integrative Biology. 2012;16(5):284-287

33. Dalakas MC. Sporadic inclusion body myositis--diagnosis, pathogenesis and therapeutic strategies. Nat Clin Pract Neurol. 2006;2(8):437-47. doi: 10.1038/ncpneuro0261.

34. Keller CW, Schmidt J, Lünemann JD. Immune and myodegenerative pathomechanisms in inclusion body myositis. Ann Clin Transl Neurol. 2017;4(6):422-445. doi: 10.1002/acn3.419.

35. Gandolfi S, Pileyre B, Drouot L, Dubus I, Auquit-Auckbur I, Martinet J. Stromal vascular fraction in the treatment of myositis. Cell Death Discov. 2023;9(1):346. doi: 10.1038/s41420-023-01605-9.

36. Kirou RA, Pinal-Fernandez I, Casal-Dominguez M, Pak K, Preusse C, Dari D, Del Orso S, Naz F, Islam S, Gutierrez-Cruz G, Naddaf E, Liewluck T, Stenzel W, Selva-O'Callaghan A, Milisenda JC, Mammen AL. Distinct cytokine and cytokine receptor expression patterns characterize different forms of myositis. Rheumatology (Oxford). 2025:keaf346. doi: 10.1093/rheumatology/keaf346.

37. Greenberg SA, Pinkus JL, Pinkus GS, Burleson T, Sanoudou D, Tawil R, Barohn RJ, Saperstein DS, Briemberg HR, Ericsson M, Park P, Amato AA. Interferon-alpha/beta-mediated innate immune mechanisms in dermatomyositis. Ann Neurol. 2005;57(5):664-78. doi: 10.1002/ana.20464.

38. Takeda Y, Tachibana I, Miyado K, Kobayashi M, Miyazaki T, Funakoshi T, Kimura H, Yamane H, Saito Y, Goto H, Yoneda T, Yoshida M, Kumagai T, Osaki T, Hayashi S, Kawase I, Mekada E. Tetraspanins CD9 and CD81 function to prevent the fusion of mononuclear phagocytes. J Cell Biol. 2003;161(5):945-56. doi: 10.1083/jcb.200212031.

39. Reyes R, Cardeñes B, Machado-Pineda Y, Cabañas C. Tetraspanin CD9: A Key Regulator of Cell Adhesion in the Immune System. Front Immunol. 2018;9:863. doi: 10.3389/fimmu.2018.00863.

40. Moos M, Tacke R, Scherer H, Teplow D, Früh K, Schachner M. Neural adhesion molecule L1 as a member of the immunoglobulin superfamily with binding domains similar to fibronectin. Nature. 1988;334(6184):701-3. doi: 10.1038/334701a0.

41. Loers G, Kleene R, Granato V, Bork U, Schachner M. Interaction of L1CAM with LC3 Is Required for L1-Dependent Neurite Outgrowth and Neuronal Survival. Int J Mol Sci. 2023;24(15):12531. doi: 10.3390/ijms241512531.

Reference Table 4S

Murgia M, Toniolo L, Nagaraj N, Ciciliot S, Vindigni V, Schiaffino S, Reggiani C, Mann M. Single Muscle Fiber Proteomics Reveals Fiber-Type-Specific Features of Human Muscle Aging. Cell Rep. 2017;19(11):2396-2409. doi: 10.1016/j.celrep.2017.05.054.

Murgia M, Nogara L, Baraldo M, Reggiani C, Mann M, Schiaffino S. Protein profile of fiber types in human skeletal muscle: a single-fiber proteomics study. Skelet Muscle. 2021;11(1):24. doi: 10.1186/s13395-021-00279-0.

Stuart CA, Stone WL, Howell ME, Brannon MF, Hall HK, Gibson AL, Stone MH. Myosin content of individual human muscle fibers isolated by laser capture microdissection. Am J Physiol Cell Physiol. 2016;310(5):C381-9. doi: 10.1152/ajpcell.00317.2015.

Maerkens A, Olivé M, Schreiner A, Feldkirchner S, Schessl J, Uszkoreit J, Barkovits K, Güttsches AK, Theis V, Eisenacher M, Tegenthoff M, Goldfarb LG, Schröder R, Schoser B, van der Ven PF, Fürst DO, Vorgerd M, Marcus K, Kley RA. New insights into the protein aggregation pathology in myotilinopathy by combined proteomic and immunolocalization analyses. Acta Neuropathol Commun. 2016;4:8. doi: 10.1186/s40478-016-0280-0.

Ubaida-Mohien C, Lyashkov A, Gonzalez-Freire M, Tharakan R, Shardell M, Moaddel R, Semba RD, Chia CW, Gorospe M, Sen R, Ferrucci L. Discovery proteomics in aging human skeletal muscle finds change in spliceosome, immunity, proteostasis and mitochondria. Elife. 2019;8:e49874. doi: 10.7554/eLife.49874.

Güttsches, AK, Brady, S, Krause, K, Maerkens, S, Uszkoreit, J, Eisenacher, M, Schreiner, A, Galozzi, S, Mertens-Rill, J, Tegenthoff, M, Holton, JL, Harms, MB, Lloyd, TE, Vorgerd, M, Weihl, CC, Marcus, K, Kley, RA. Proteomics of rimmed vacuoles define new risk allele in inclusion body myositis. Ann Neurol.2017;81: 227-239. https://doi.org/10.1002/ana.24847

Güttsches AK, Jacobsen F, Schreiner A, et al. Chaperones in sporadic inclusion body myositis—Validation of proteomic data. Muscle Nerve. 2020;61:116–121. https://doi.org/10.1002/mus.26742

Roos A, Preusse C, Hathazi D, Goebel HH, Stenzel W. Proteomic Profiling Unravels a Key Role of Specific Macrophage Subtypes in Sporadic Inclusion Body Myositis. Front Immunol. 2019;10:1040. doi: 10.3389/fimmu.2019.01040.

Pattamaprapanont P, Cooney EM, MacDonald TL, Paulo JA, Pan H, Dreyfuss JM, Lessard SJ. Matrisome proteomics reveals novel mediators of muscle remodeling with aerobic exercise training. Matrix Biol Plus. 2024;23:100159. doi: 10.1016/j.mbplus.2024.100159.

Peterson JM, Leclair V, Oyebode OE, Herzallah DM, Nestor-Kalinoski AL, Morais J, Zahedi RP, Alamr M, Di Battista JA, Hudson M. A window into intracellular events in myositis through subcellular proteomics. Inflamm Res. 2025;74(1):31. doi: 10.1007/s00011-025-01996-8.

Moriggi M, Torretta E, Cescon M, Russo L, Gregorio I, Braghetta P, Sabatelli P, Faldini C, Merlini L, Gargioli C, Bonaldo P, Gelfi C, Capitanio D. Characterization of Proteome Changes in Aged and Collagen VI-Deficient Human Pericyte Cultures. Int J Mol Sci. 2024;25(13):7118. doi: 10.3390/ijms25137118

Deshmukh AS, Murgia M, Nagaraj N, Treebak JT, Cox J, Mann M. Deep proteomics of mouse skeletal muscle enables quantitation of protein isoforms, metabolic pathways, and transcription factors. Mol Cell Proteomics. 2015;14(4):841-53. doi: 10.1074/mcp.M114.044222

ProteomeXchange Consortium:
Deutsch EW, Bandeira N, Perez-Riverol Y, Sharma V, Carver J, Mendoza L, Kundu DJ, Wang S, Bandla C, Kamatchinathan S, Hewapathirana S, Pullman B, Wertz J, Sun Z, Kawano S, Okuda S, Watanabe Y, MacLean B, MacCoss M, Zhu Y, Ishihama Y and Vizcaíno JA. The ProteomeXchange Consortium at 10 years: 2023 update. Nucleic Acids Res. 2023; 51(D1): D1539–D1548.